




RESEARCH ARTICLE

Prescribed performance LOS guidance-based dynamic surface path following control of surface vessel with position and heading errors constraint

Zhipeng Shen, Ang Li, Li Li, and Haomiao Yu* 

College of Marine Electrical Engineering, Dalian Maritime University, Dalian, People's Republic of China.

*Corresponding author. Haomiao Yu; E-mail: yuhaomiao1983@163.com

Received: 26 July 2021; **Accepted:** 12 March 2023; **First published online:** 18 April 2023

Keywords: barrier Lyapunov function; prescribed performance; line-of-sight; path following; surface vessel

Abstract

Concentrating on a surface vessel with input saturation, model uncertainties and unknown disturbances, a path following the adaptive backstepping control method based on prescribed performance line-of-sight (PPLOS) guidance is proposed. First, a prescribed performance asymmetric modified barrier Lyapunov function (PPAMBLF) is used to design the PPLOS and the heading controller, which make the path following position and heading errors meet the prescribed performance requirements. Furthermore, the backstepping and dynamic surface technique (DSC) are used to design the path following controller and the adaptive assistant systems are constructed to compensate the influence of input saturation. In addition, neural networks are introduced to approximate model uncertainties, and the adaptive laws are designed to estimate the bounds of the neural network approximation errors and unknown disturbances. According to the Lyapunov stability theory, all signals are semi-globally uniformly ultimately bounded. Finally, a 76·2 m supply surface vessel is used for simulation experiments. The experimental results show that although the control inputs are limited, the control system can still converge quickly, and both position and heading errors can be limited to the prescribed performance requirements.

1. Introduction

In recent years, manned and unmanned vessels (Naus et al., 2021; Rutkowski, 2021; Specht et al., 2021) have played a key role in various ocean engineering such as maritime rescue, ocean exploration (Liang et al., 2017; Stateczny et al., 2021) and resource development. Ship motion control has received widespread attention to meet the needs of different tasks, realise the intelligence and automation of ships, and ensure the safety and economy of ships. The research on ships in recent years includes path planning (Lyu and Yin, 2019), collision avoidance (Li and Zheng, 2020; Xu et al., 2020) and track control. Track control is divided into trajectory tracking and path following. Trajectory tracking (Wang and Su, 2021) is strictly constrained by time, enabling the ship to track the desired trajectory in real-time; Path following (Nie et al. 2021) is not subject to time requirements, it only needs to track the geometric position of the target path. In actual ship navigation, it generally not needed to arrive at the designated location at a specific time, so ship path following is more extensive. In some special marine engineering operations, such as engineering drilling platforms and engineering experimental ships which require a high degree of freedom, the control performance of underactuated ships (Hou et al., 2020; Xie et al., 2020; Zhang et al., 2020) can no longer meet the engineering requirements. Therefore, the fully actuated (Zheng et al., 2018a; Del-Rio-Rivera et al., 2020) path following surface vessel with higher degree of freedom and stronger performance has great research value and significance.

Aimed at the problem of surface vessel path following control, the main methods include the Serret–Frenet (SF) frame (Liu et al., 2017), logical virtual ship (LVS) guidance (Zhang et al., 2015), line-of-sight (LOS) guidance and so on. The LOS guidance can reduce the output dimension of the system and greatly simplify the design of the path following controller. The LOS-based surface vessel path following control system is composed of a kinematics-level LOS guidance control system and a dynamics-level heading and speed tracking control system. The former provides a heading guidance angle for the surface vessel by designing a guidance law, and the latter designs a heading and velocity tracking controller to realise the surface vessel can follow the desired path at a certain desired speed. LOS guidance has been extensively studied and applied by many researchers in different aspects. These LOS guidance can be divided into three main categories. The first category is compensation for sideslip angle and disturbance. The integral LOS (ILOS) (Lekkas and Fossen, 2014) guidance method introduces an integrator based on the traditional LOS, which can compensate for the influence of constant sideslip angle on the path following control system. Zhang et al. (2019) applied ILOS and a robust adaptive algorithm to the path following control of an unmanned robot sailboat. Adaptive integral LOS (AILOS) (Fossen and Lekkas, 2017) adds an adaptive rate to the ILOS guidance. It overcomes the impact of unknown sideslip angles and unknown time-varying ocean currents in kinematics on the system and enhances the robustness of the system. Predictor-based LOS (PLOS) (Liu et al., 2016b) introduces the predictor into the design of LOS guidance. This guidance uses a predictor to estimate the unknown constant drift angle to improve the accuracy of the sideslip angle estimation. However, the sideslip angle involved in the above method is constant or slowly time-varying, and it does not solve the problem of time-varying sideslip angle. Extended state observer-based LOS (ELOS) (Liu et al., 2016a) based on extended state observers (ESOs) solves the problem of time-varying sideslip angle. A real ship simulation can be used to verify the feasibility of the guidance. The second category is to optimise parameters such as lookahead distance and desired velocity in LOS guidance. Lekkas and Fossen (2014) presented the forward distance that varies with the cross-track error in ILOS guidance. When the ship is far from the desired path, a smaller forward distance is obtained, which will make the bow of the ship more perpendicular to the desired path and increase the error rate. Surge-guided LOS (SGLOS) (Wang et al., 2019) is designed with a time-varying speed that varies with the lateral error. Compared with the traditional single constant speed, this guidance method has a faster convergence speed and is more reasonable. The third category is to constrain the tracking error. In actual navigation, especially in complex sea conditions or narrow waters, if the navigation path and tracking error of the ship are not restricted, there will be great safety hazards. Zheng and Feroskhan (2017) used the logarithmic error transformed functions to construct the LOS guidance. This guidance can convert performance constraints into an equivalent unrestricted range, ensuring the prescribed performance in the path following process. Zheng et al. (2018b) proposed error-constrained LOS (ECLOS) guidance based on the barrier Lyapunov function (BLF), and used the tan-type BLF to limit the steady-state performance of the surface vessel in path following.

The heading and velocity control part of path following is similar to the principle of trajectory tracking. At present, the common controller design methods include backstepping control, fuzzy control, sliding mode control, robust control and so on. Among them, Fossen and Berge (1997) first proposed the backstepping and applied it to ship control, by constructing the Lyapunov function to inverse the controller. Because of its simple and direct design, it has been studied by many researchers. Swaroop et al. (2000) added the dynamic surface control technique (DSC) to the backstepping, which avoids the ‘differential explosion’ caused by the derivation of the virtual control rate in backstepping and simplifies the computational complexity. In actual sea conditions, unknown disturbances such as wind, waves and currents are inevitable. Additionally, the weight of the ship may change with the load, so the ship may have model uncertainties. Shen et al. (2018) used neural networks with adaptive laws to construct a fully actuated surface vessel trajectory tracking controller, which can not only approximate the model uncertainties and unknown disturbances, but also effectively improve the robustness of the system. Shen et al. (2020b) proposed a finite-time observer, which can observe unmeasurable speed values and unknown interference within a limited time. This method simultaneously solves the problem of an unmeasurable system state and unknown disturbances. Although the theoretical research results on

unknown disturbances and model uncertainties are fruitful, few researchers have considered the physical constraints of a surface vessel in actual navigation.

On the one hand, the surface vessel itself has the problem of input saturation. For example, the torque generated by the rudder and propeller cannot be infinite. When the input signal of the actuator is too large, saturation will occur. The most direct result will make the ship unable to track the desired path or even cause the system to oscillate and become unbalanced. For a class of nonlinear systems with input saturation, Chen et al. (2011) proposed constraint adaptive control and designed a command filter controller (CFC). It can not only solve the problem of system input saturation, but also solve the problem of 'differential explosion' caused by the backstepping method. By virtue of constructing an auxiliary dynamic system to deal with output saturation, Du et al. (2016) designed a robust nonlinear controller for ship dynamic positioning, which effectively solves the impact of limited output on the system. Shen et al. (2020a) introduced the smooth Nussbaum function to construct the auxiliary system, which has the property that the upper and lower bound integrals tend to infinity. This auxiliary system can well compensate the nonlinear part caused by the input saturation. Shen et al. (2020b) and Yang and Chen (2016) apply an adaptive auxiliary system to overcome the influence of input saturation on the system, which can make the system stable in the presence of input saturation. Compared with that used by Shen et al. (2020a), this adaptive auxiliary system is simpler.

On the other hand, from the external water environment, a surface vessel may be affected by the output constraint. In narrow waterways or specific engineering operations, it is forbidden for ships to have large path following errors in path following, so it is necessary to limit the output of the system. At present, the methods to solve the output constraint include the prescribed performance function (PPF) and the barrier Lyapunov function (BLF). Bechlioulis and Rovithakis (2008) first proposed the prescribed performance control method. Through the error transformed function constructed by PPF, the constrained performance is converted to the equivalent unconstrained range. Jia et al. (2019) combined the prescribed performance with the backstepping and designed an underactuated trajectory tracking controller with preset performance. However, obtaining the inverse function of the logarithmic error transformed function is very complicated, which is not convenient for the design of the controller, and will lead to the singularity of the system. To solve this problem, Li et al. (2019) improved the error transformed function based on the work of Jia et al. (2019), and proposed a non-logarithmic error transformed function, which effectively simplified the complexity of system design. The prescribed performance function can constrain the steady-state and transient performance of the system, but it has the disadvantages of poor scalability, sensitivity to the initial position and complicated controller design. The BLF is an improvement on the Lyapunov function. Compared with the error transformed function, the BLF solves the problem of output constraint more directly. BLF starts directly from the starting point (Lyapunov function) of the controller design, and directly constrains the error by constructing an appropriate BLF. This method does not need to convert the errors, thus simplifying the controller design and solving the singularity problem. Xu and Jin (2013) proposed a tangential barrier Lyapunov function (TBLF), which is used for the design of a multi-input multi-output nonlinear control system with output constraints. However, when deriving the TBLF, the denominator contains a trigonometric function term, which complicates the design of the controller. Zhao et al. (2014) used the symmetric barrier Lyapunov function (SBLF) to solve the problem of trajectory tracking of the ship with input constraints. Since the SBLF is the logarithmic form, the derivative is the regular fractional form, which can solve the problem of increased complexity of the system caused by the time derivative of the trigonometric function term. However, the initial restricted area of the SBLF is symmetrical, and the upper and lower bounds of the output constraints may not be the same in the system, which makes the SBLF have great limitations. To solve this problem, Qiu et al. (2015) proposed the asymmetric barrier Lyapunov function (ABLF) to solve a problem of a class of nonlinear systems with output constraints. The ABLF relaxes the restriction that the initial restricted area must be symmetrical. However, in special cases, such as when the constraint boundary approaches infinity, no matter how large the error is, the traditional ABLF approaches zero, which cannot be used as a basis for judging the stability of the system. Chen et al. (2020) first proposed the asymmetric modified barrier Lyapunov function (AMBLF) to realise the

full-state constrained control of spacecraft. AMBLF is an improvement of the traditional ABLF. When the constraint boundary is infinite, the AMBLF can be transformed into a traditional quadratic BLF by using L'Hospital's rule, which makes the AMBLF more general. However, in the above literature (Xu and Jin, 2013; Zhao et al., 2014; Qiu et al., 2015; Chen et al., 2020), the BLF can only realise the steady-state constraints of the system, and cannot achieve dynamic constraints and improve the steady-state constraint's transient performance of the system.

Inspired by the above research, to efficiently complete complex and accurate engineering tasks, we propose a BLF-based surface vessel path following controller which is suitable for model uncertainties, unknown disturbances, input saturation and prescribed performance. The main contributions and innovations of this paper are summarised.

- (i) We propose the prescribed performance asymmetric modified barrier Lyapunov function (PPAMBLF). Compared with the traditional AMBLF (Chen et al., 2020), the PPAMBLF is a combination of the AMBLF and PPF, which can not only constrain the steady-state performance of the system, but also has the prescribed performance characteristics of the PPF.
- (ii) This paper proposes the prescribed performance line-of-sight (PPLOS) guidance law for the first time. PPLOS guidance is based on the PPAMBLF, which can ensure that the tracking errors of the path following kinematics guidance part converge within the expected constraint range in real-time, ensuring the prescribed performance of the guidance system. Compared with ECLOS (Zheng et al., 2018b), PPLOS has three obvious advantages: (1) PPLOS avoids the complexity of the system caused by the trigonometric function term of the TBLF; (2) PPLOS can make the restricted area asymmetric, which is more general; (3) PPLOS can not only meet the steady-state constraints of the guidance system, but also meet its transient performance.
- (iii) Zheng et al. (2018b) and Zheng and Feroskhan (2017) only limited the position error of the ship by designing guidance in kinematics, and did not restrict the error between the heading guidance angle and the actual heading angle in dynamics. In this paper, the PPAMBLF is further applied to the heading control of ship path following, so that the heading error can also meet the prescribed performance requirements and the tracking accuracy of the system is further enhanced.
- (iv) This paper constructs a fully actuated surface vessel path following controller based on PPLOS, introduces the adaptive assistant systems to compensate for the impact of input saturation, uses RBF neural networks to approximate the model uncertainties, and designs adaptive laws to estimate the bounds of the neural network approximation errors and unknown external environmental disturbances. Finally, combining the backstepping, DSC and PPAMBLF, we design a surface vessel path following adaptive backstepping control with prescribed performance and input saturation.

The specific arrangement of the paper is as follows: Section 1 provides an introduction; Section 2 includes the problem description and preliminary work; Section 3 presents the design of the surface vessel path following controller; Section 4 gives the strict stability proof; Section 5 carries out MATLAB simulation, and analyses the experimental result; and Section 6 includes the conclusions.

2. Problem description and preliminaries

2.1. Problem description

2.1.1. Surface vessel model

Figure 1 shows the surface vessel motion. In this paper, we define the inertial reference frame (IRF) as $O_E - X_E Y_E$ and the body-fixed reference frame (BRF) as $O - XY$. Considering the three-degrees-of-freedom surface vessel in the presence of model uncertainties and external disturbances, the nonlinear mathematical model (Shen et al., 2020a; Wang et al., 2021) for a surface vessel can be expressed as

$$\dot{\eta} = J(\psi)v \quad (2.1a)$$

$$M\dot{v} + C(v)v + Dv + \Delta f = \text{sat}(\tau) + d \quad (2.1b)$$

where $\eta = [x, y, \psi]^T$ is the surface vehicle position vector in the earth-fixed frame, where (x, y) is the surface vehicle actual position and ψ is the heading angle; $\mathbf{v} = [u, v, r]^T$ is the velocity vector in the body-fixed frame, consisting of surge u , sway v and yaw r ; $\Delta \mathbf{f} = [\Delta f_u, \Delta f_v, \Delta f_r]$ are the uncertainties of the surface vessel model; $\mathbf{d} = [d_u, d_v, d_r]^T$ is the unknown external environmental disturbance; $\mathbf{J}(\psi)$ is the rotation matrix; \mathbf{M} is the positive definite inertia matrix including the vessel mass and the hydrodynamic inertia; $\mathbf{C}(\mathbf{v})$ is the Coriolis centripetal; and \mathbf{D} is the damping matrix. The specific form is as follows:

$$\mathbf{J}(\psi) = \begin{bmatrix} \cos \psi & -\sin \psi & 0 \\ \sin \psi & \cos \psi & 0 \\ 0 & 0 & 1 \end{bmatrix}, \quad \mathbf{M} = \begin{bmatrix} m_{11} & 0 & 0 \\ 0 & m_{22} & 0 \\ 0 & 0 & m_{33} \end{bmatrix}$$

$$\mathbf{C}(\mathbf{v}) = \begin{bmatrix} 0 & 0 & -m_{22}v \\ 0 & 0 & m_{11}u \\ m_{22}v & -m_{11}u & 0 \end{bmatrix}, \quad \mathbf{D} = \begin{bmatrix} d_{11} & 0 & 0 \\ 0 & d_{22} & 0 \\ 0 & 0 & d_{33} \end{bmatrix}$$

$\tau = [\tau_u, \tau_v, \tau_r]$ is the actual control input consisting of surge force τ_u , sway force τ_v , and yaw moment τ_r . Considering the input saturation, $\text{sat}(\tau)$ is the system input subject to saturation, and the specific description is as follows:

$$\text{sat}_i(\tau_i) = \begin{cases} \tau_i^+, & \text{if } \tau_i > \tau_i^+ \\ \tau_i, & \text{if } \tau_i^- \leq \tau_i \leq \tau_i^+ \\ \tau_i^-, & \text{if } \tau_i < \tau_i^- \end{cases} \quad (i = u, v, r) \tag{2.2}$$

where $\tau_i^+ > 0, \tau_i^- < 0$ are the maximum and the minimum control force or moment of the surface vessel path following control system. Let $\Delta \tau_i = \text{sat}_i(\tau_i) - \tau_i, i = u, v, r$. We can expand Equation (2.1b) as

$$\begin{cases} \dot{u} = \frac{1}{m_{11}}(m_{22}vr - d_{11}u - \Delta f_u) + \frac{\text{sat}_u(\tau_u) + d_u}{m_{11}} \\ \dot{v} = \frac{1}{m_{22}}(-m_{11}ur - d_{22}v - \Delta f_v) + \frac{\text{sat}_v(\tau_v) + d_v}{m_{22}} \\ \dot{r} = \frac{1}{m_{33}}((m_{11} - m_{22})uv - d_{33}r - \Delta f_r) + \frac{\text{sat}_r(\tau_r) + d_r}{m_{33}} \end{cases} \tag{2.3}$$

Assumption 1. The disturbance of the external environment experienced by the surface vessel is unknown, but the disturbance is bounded, and its rate of change is also bounded, that is, $\|\dot{d}(t)\| \leq C_d < \infty$.

Assumption 2. The parameter matrices $\mathbf{M}, \mathbf{C}(\mathbf{v})$ and \mathbf{D} of the surface vessel model are known. In addition, the model uncertainties are unknown but bounded.

2.1.2. Control objective

The surface vessel’s LOS guidance method is shown in Figure 2. We define the path reference frame (PRF) as $O_p - X_p Y_p$. Then the desired path to be followed is defined as $\eta_p(\theta) = [x_p(\theta), y_p(\theta)]$, where $\eta_p(\theta)$ is the desired path parameter, and $\psi_p(\theta)$ is the path-tangent angle of the desired path, defined as $\psi_p(\theta) = \arctan 2(y'_p(\theta), x'_p(\theta))$.

Remark 1. For $(\cdot)'_p(\theta)$, we have $(\cdot)'_p(\theta) \triangleq d(\cdot)_p/d\theta$.

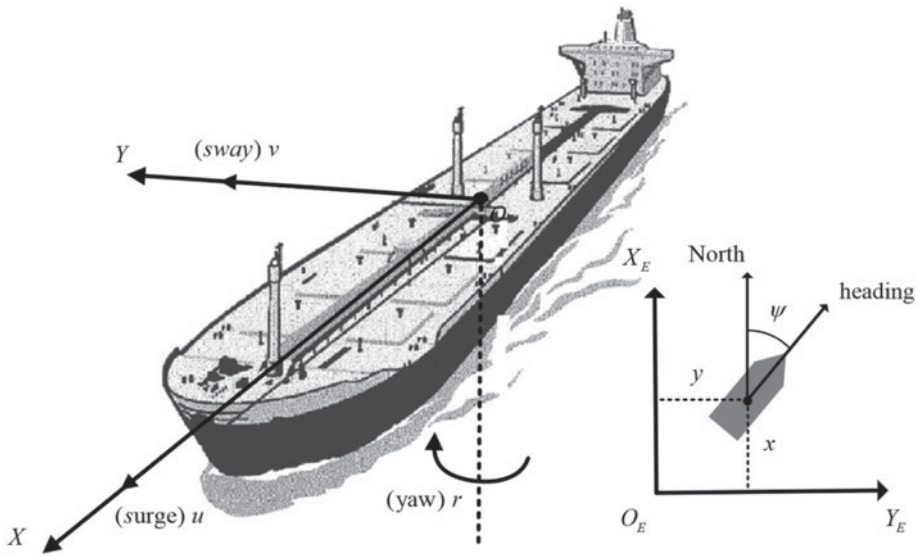


Figure 1. Motion of surface vessel.

For the surface vessel with positions, the along-tracking error and cross-tracking error (as shown in Figure 2) of the position in the IRF can be expressed in the PRF as

$$\begin{bmatrix} x_e \\ y_e \end{bmatrix} = \begin{bmatrix} \cos \psi_p & -\sin \psi_p \\ \sin \psi_p & \cos \psi_p \end{bmatrix}^T \begin{bmatrix} x - x_p \\ y - y_p \end{bmatrix} \tag{2.4}$$

The derivative of x_e is

$$\begin{aligned} \dot{x}_e &= \underbrace{\dot{x} \cos \psi_p + \dot{y} \sin \psi_p}_{a_1} - \underbrace{\dot{x}_p \cos \psi_p - \dot{y}_p \sin \psi_p}_{a_2} \\ &\quad + \underbrace{\dot{\psi}_p (-x - x_p) \sin \psi_p + (y - y_p) \cos \psi_p}_{\text{cross-tracking error } (y_e)} \end{aligned} \tag{2.5}$$

According to Equation (2.1a), the a_1 and a_2 in Equation (2.5) can be further rewritten as

$$a_1 = U \cos(\psi - \psi_p + \beta) \tag{2.6a}$$

$$a_2 = \dot{\theta} \sqrt{x_p'^2(\theta) + y_p'^2(\theta)} \cos(\psi_p + \phi) \tag{2.6b}$$

where $U = \sqrt{u^2 + v^2} \geq 0$ is the actual velocity of the surface vessel, $\beta = \arctan2(v, u)$ is the sideslip angle (as shown in Figure 2) and $\phi = \arctan2(-y'_d(\theta), -x'_d(\theta)) = -\psi_d$.

Because the simplification of \dot{x}_e and \dot{y}_e are similar, the derivative of the tracking errors become

$$\begin{cases} \dot{x}_e = U \cos(\psi - \psi_p + \beta) + \dot{\psi}_p y_e - \dot{\theta} \sqrt{x_p'^2(\theta) + y_p'^2(\theta)} \\ \dot{y}_e = U \sin(\psi - \psi_p + \beta) - \dot{\psi}_p x_e \end{cases} \tag{2.7}$$

where $\dot{\psi}_p = ((-x_p'' y_p' + y_p'' x_p') / (x_p'^2 + y_p'^2)) \dot{\theta}$.

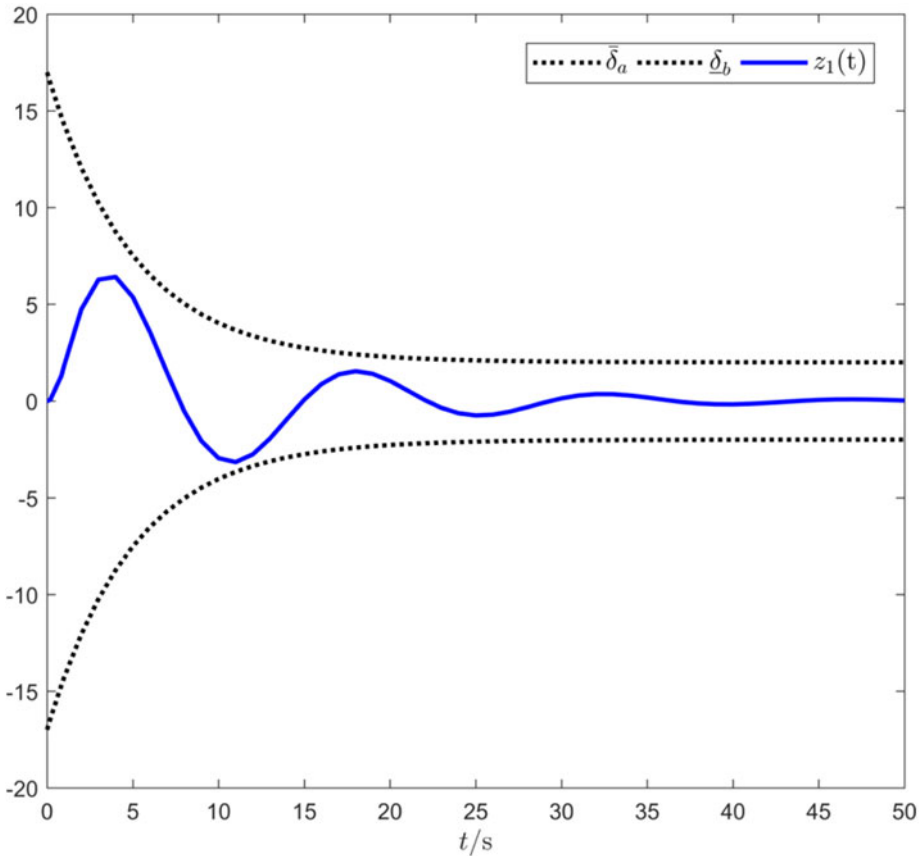


Figure 3. Pictorial illustration of prescribed performance.

2.3. Barrier Lyapunov function

2.3.1. Asymmetric modified barrier Lyapunov function

The asymmetric modified barrier Lyapunov function (AMBLF) (Chen et al., 2020) can be expressed as

$$V_b = \frac{q(z(t))}{2} \ln \frac{k_a^2 e^{z(t)^2}}{k_a^2 - z(t)^2} + \frac{1 - q(z(t))}{2} \ln \frac{k_b^2 e^{z(t)^2}}{k_b^2 - z(t)^2} \tag{2.9}$$

where $z(t)$ is the variable that needs to be constrained, which generally is the systematic error. We define $k_a = k_c - Y_0$, $k_b = k_d - Y_0$. Here, $k_c > 0$, $k_d > 0$ are the upper and lower bounds of constant value constraints, and Y_0 is the expected value. Hence, $-k_b < z(0) < -k_a$, $q(*) = \begin{cases} 1, & * > 0 \\ 0, & * \leq 0 \end{cases}$.

Remark 2. Through simple calculations, we can get $V_b(0^+) = V_b(0^-) = 0$, $\lim_{z \rightarrow 0^+} dV_b/dz = \lim_{z \rightarrow 0^-} dV_b/dz = 0$, which explain that V_b is a continuous derivable function.

Remark 3. When $k_a \rightarrow \infty, k_b \rightarrow \infty$, $\lim_{k_a \rightarrow \infty} \frac{1}{2} \ln(k_a^2 e^{z^2} / (k_a^2 - z^2)) = \lim_{k_b \rightarrow \infty} \frac{1}{2} \ln(k_b^2 e^{z^2} / (k_b^2 - z^2)) = \frac{1}{2} z^2$ can be obtained using L'Hospital's rule. That is, when the system is unconstrained, the AMBLF can be converted to a general quadratic Lyapunov function.

2.3.2. Prescribed performance symmetric modified barrier Lyapunov function

To ensure that the surface vessel path following position errors meet the prescribed performance requirements, we further improve the AMBLF. We combine the PPF with AMBLF to design the

PPAMBLF, which can make the system meet the steady-state performance and transient performance. For compact $Z = \{z(t) : -\underline{\delta}_a < z(t) < \bar{\delta}_b\}$, there are the following equations:

$$V_b = \frac{q(z(t))}{2} \ln \frac{\bar{\delta}_a(t)^2 e^{z(t)^2}}{\bar{\delta}_a(t)^2 - z(t)^2} + \frac{1 - q(z(t))}{2} \ln \frac{\underline{\delta}_b(t)^2 e^{z(t)^2}}{\underline{\delta}_b(t)^2 - z(t)^2} \tag{2.10}$$

where, $\bar{\delta}(t)$ and $\underline{\delta}(t)$ are the prescribed performance functions such as in Equation (2.8).

Remark 4. Finding the value of the function on both sides of the zero point of the PPAMBLF and its first derivative, we can get $V_b(0^+) = V_b(0^-) = 0$, $\lim_{z(t) \rightarrow 0^+} dV_b/dz(t) = \lim_{z(t) \rightarrow 0^-} dV_b/dz(t) = 0$. That is, the PPAMBLF is a continuous derivative function.

Theorem 1. From Chen et al. (2020), we can get the following inequality:

$$\frac{1}{2} \left(1 + \frac{q(z)}{K_a^2 - z^2} + \frac{1 - q(z)}{K_b^2 - z^2} \right) z^2 \geq V_b \tag{2.11}$$

where $-k_a < z(t) < k_b$.

Let $K_a = \bar{\delta}_a$, $K_b = \underline{\delta}_b$. Because $\bar{\delta}_a$ and $\underline{\delta}_b$ have no direct functional relationship with z , we can obtain

$$\frac{1}{2} \left(1 + \frac{q(z)}{\bar{\delta}_a^2 - z^2} + \frac{1 - q(z)}{\underline{\delta}_b^2 - z^2} \right) z^2 \geq V_b \tag{2.12}$$

Remark 5. When $\bar{l}_a \rightarrow 0$, $l_b \rightarrow 0$, limiting to the prescribed performance functions, we can get $\lim_{\bar{l}_a \rightarrow 0} \bar{\delta}_a(t) = \delta_{a,\max}$, $\lim_{l_b \rightarrow 0} \underline{\delta}_b(t) = \delta_{b,\min}$. That is, the PPAMBLF proposed in this paper can be simplified to the AMBLF. On this basis, we continue to let $\delta_{a,\max} = \delta_{b,\min} = \infty$, so the PPAMBLF proposed can be simplified to the general quadratic Lyapunov function.

Remark 6. A conventional AMBLF can only guarantee the steady-state performance of the system. While ensuring steady-state performance, the PPAMBLF further restricts the transient performance of the system according to the prescribed performance function. the PPAMBLF can ensure that the system has a better tracking effect in the initial and mid-stage tracking. The specific performance is shown in the intermediate time period from the start of the path following of the system ($t = 0$) to the steady-state stage of the expected path ($t = t_0$).

3. Design of surface vessel path following controller

Assuming that there are input saturation, model uncertainties, unknown disturbances and all the states of the surface vessel are measurable, we first design the PPLOS guidance, which enables the surface vessel’s position tracking errors to meet the consistent asymptotic stability while remaining within the prescribed performance constraints. The PPAMBLF is further used to constrain the heading of the surface vessel, so that the heading error also meets the prescribed performance requirements. We use backstepping and DSC to design the heading control system and velocity control system. The adaptive assistant systems are used to compensate for input saturation. Neural networks are introduced to approximate the model uncertainties. The adaptive laws are designed to estimate the bounds of the neural network approximation errors and the unknown. This method achieves the following control objectives: (1) the surface vessel can track the desired path and meet the prescribed performance; (2) the surface vessel can reach the desired velocity and maintain it; (3) all signals in the system are consistent asymptotic stability. A block diagram of the control system is shown in Figure 4.

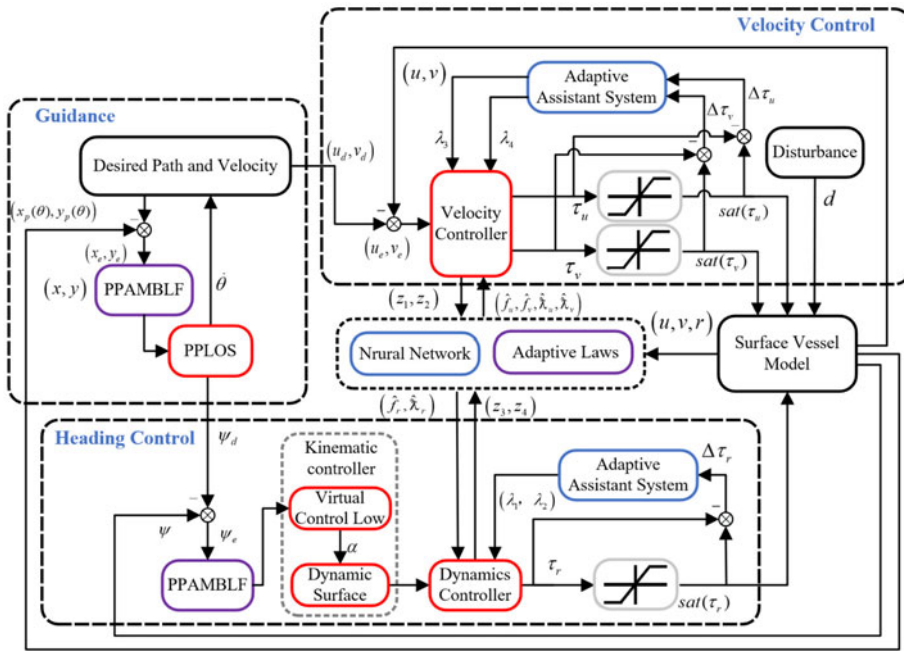


Figure 4. Block diagram of the control system.

3.1. PPLOS guidance

We introduce the PPAMBLF to the along-track error x_e and the across-track error y_e as follows:

$$\begin{aligned}
 V_1 = & \frac{1}{2} \left(\underbrace{q(x_e) \ln \frac{\bar{\delta}_{a1}^2 e^{x_e^2}}{\bar{\delta}_{a1}^2 - x_e^2} + (1 - q(x_e)) \ln \frac{\bar{\delta}_{b1}^2 e^{x_e^2}}{\bar{\delta}_{b1}^2 - x_e^2}}_{\text{section of } x_e} \right) \\
 & + \frac{1}{2} \left(\underbrace{q(y_e) \ln \frac{\bar{\delta}_{c1}^2 e^{y_e^2}}{\bar{\delta}_{c1}^2 - y_e^2} + (1 - q(y_e)) \ln \frac{\bar{\delta}_{d1}^2 e^{y_e^2}}{\bar{\delta}_{d1}^2 - y_e^2}}_{\text{section of } y_e} \right)
 \end{aligned} \tag{3.1}$$

where $\bar{\delta}_{a1}, \bar{\delta}_{b1}, \bar{\delta}_{c1}, \bar{\delta}_{d1}$ are prescribed performance functions, $q(*) = \begin{cases} 1, & \text{if } * > 0 \\ 0, & \text{if } * \leq 0 \end{cases}$

$$\begin{aligned}
 \dot{V}_1 = & \left(1 + \frac{q(x_e)}{\bar{\delta}_{a1}^2 - x_e^2} + \frac{1 - q(x_e)}{\bar{\delta}_{b1}^2 - x_e^2} \right) x_e \dot{x}_e \\
 & + \left(1 + \frac{q(y_e)}{\bar{\delta}_{c1}^2 - y_e^2} + \frac{1 - q(y_e)}{\bar{\delta}_{d1}^2 - y_e^2} \right) y_e \dot{y}_e \\
 & - \frac{q(x_e) x_e^2 \dot{\bar{\delta}}_{a1}}{\bar{\delta}_{a1} (\bar{\delta}_{a1}^2 - x_e^2)} - \frac{(1 - q(x_e)) x_e^2 \dot{\bar{\delta}}_{b1}}{\bar{\delta}_{b1} (\bar{\delta}_{b1}^2 - x_e^2)} \\
 & - \frac{q(y_e) y_e^2 \dot{\bar{\delta}}_{c1}}{\bar{\delta}_{c1} (\bar{\delta}_{c1}^2 - y_e^2)} - \frac{(1 - q(y_e)) y_e^2 \dot{\bar{\delta}}_{d1}}{\bar{\delta}_{d1} (\bar{\delta}_{d1}^2 - y_e^2)}
 \end{aligned} \tag{3.2}$$

Together with Equations (2.7) and (3.2), we have

$$\begin{aligned} \dot{V}_1 &= \xi_{11}x_e(U \cos(\psi - \psi_p + \beta) - \dot{\theta}\vartheta) \\ &\quad + \xi_{12}y_e(U \sin(\psi - \psi_p + \beta)) \\ &\quad + \varpi_{11}x_e^2 + \varpi_{12}y_e^2 \end{aligned} \tag{3.3}$$

where ξ_{12} , ϖ_{11} , ϖ_{12} , ϑ are as follows:

$$\begin{cases} \xi_{11} = 1 + \frac{q(x_e)}{\bar{\delta}_{a1}^2 - x_e^2} + \frac{1 - q(x_e)}{\underline{\delta}_{b1}^2 - x_e^2} \\ \xi_{12} = 1 + \frac{q(y_e)}{\bar{\delta}_{c1}^2 - y_e^2} + \frac{1 - q(y_e)}{\underline{\delta}_{d1}^2 - y_e^2} \\ \varpi_{11} = -\left(\frac{q(x_e)\dot{\bar{\delta}}_{a1}}{\bar{\delta}_{a1}(\bar{\delta}_{a1}^2 - x_e^2)} + \frac{(1 - q(x_e))\dot{\underline{\delta}}_{b1}}{\underline{\delta}_{b1}(\underline{\delta}_{b1}^2 - x_e^2)} \right) \\ \varpi_{12} = -\left(\frac{q(y_e)\dot{\bar{\delta}}_{c1}}{\bar{\delta}_{c1}(\bar{\delta}_{c1}^2 - y_e^2)} + \frac{(1 - q(y_e))\dot{\underline{\delta}}_{d1}}{\underline{\delta}_{d1}(\underline{\delta}_{d1}^2 - y_e^2)} \right) \end{cases} \tag{3.4a}$$

$$\begin{aligned} \vartheta &= \sqrt{x_p'^2(\theta) + y_p'^2(\theta)} \\ &\quad - y_e \frac{-x_p''y_p' + y_p''x_p'}{x_p'^2 + y_p'^2} \left(1 - \frac{1 + \frac{q(y_e)}{\bar{\delta}_{c1}^2 - y_e^2} + \frac{1 - q(y_e)}{\underline{\delta}_{d1}^2 - y_e^2}}{1 + \frac{q(x_e)}{\bar{\delta}_{a1}^2 - x_e^2} + \frac{1 - q(x_e)}{\underline{\delta}_{b1}^2 - x_e^2}} \right) \end{aligned} \tag{3.4b}$$

Remark 7. Because $-\underline{\delta}_{b1} < x_e < \bar{\delta}_{a1}$, when $0 < x_e$, we can get $\xi_{11} = 1 + 1/(\bar{\delta}_{a1}^2 - x_e^2) \geq 1 > 0$, and when $x_e \leq 0$, we can get $\xi_{11} = 1 + 1/(\underline{\delta}_{b1}^2 - x_e^2) \geq 1 > 0$. In summary, $\xi_{11} > 0$, and by the same token, $\xi_{12} > 0$.

We design the desired heading angle ψ_d and the update law of θ as

$$\psi_d = \psi_p(\theta) + \arcsin\left(\frac{-k_\Delta y_e}{\sqrt{1 + (k_\Delta y_e)^2}}\right) - \beta \tag{3.5a}$$

$$\dot{\theta} = \frac{U \cos(\psi - \psi_d + \beta) + (k_\theta - (\varpi_{12}y_e^2/x_e + \varpi_{11}))/\xi_{11}x_e}{\vartheta} \tag{3.5b}$$

Assumption 5. Since the design of the guidance law is based on kinematics and does not consider the dynamics, we assume the actual heading angle ψ of the surface vessel can perfectly track the desired heading angle ψ_d given by the guidance. That is, $\psi = \psi_d$.

3.2. Heading tracking control

To compensate for the impact of input saturation, we introduce a second-order adaptive assistant system (Yang and Chen, 2016; Shen et al., 2020b):

$$\begin{cases} \dot{\lambda}_1 = -\hbar_1 \lambda_1 + \lambda_2 \\ \dot{\lambda}_2 = -\hbar_2 \lambda_2 + \frac{1}{m_{33}} \Delta \tau_r \end{cases} \tag{3.6}$$

where $\bar{h}_1, \bar{h}_2 > 0$ are design constants, λ_1, λ_2 are auxiliary variables. The heading error z_1 and yaw error of z_2 of the surface vessel are given as

$$\begin{cases} z_1 = \psi - \psi_d - \lambda_1 \\ z_2 = r - r_d - \lambda_2 \end{cases} \tag{3.7}$$

Step 1: According to z_2 , the time derivation of z_1 is

$$\dot{z}_1 = z_2 + r_d + \lambda_2 - \dot{\psi}_d - \dot{\lambda}_1 \tag{3.8}$$

To ensure the prescribed performance of the system, we introduce the PPAMBLF of z_1 as

$$V_2 = \frac{1}{2} \left(q(z_1) \ln \frac{\bar{\delta}_{a2}^2 e^{z_1^2}}{\bar{\delta}_{a2}^2 - z_1^2} + (1 - q(z_1)) \ln \frac{\underline{\delta}_{b2}^2 e^{z_1^2}}{\underline{\delta}_{b2}^2 - z_1^2} \right) \tag{3.9}$$

where $\bar{\delta}_{a2}(t) > z_1(0) > -\underline{\delta}_{b2}(t)$, $\bar{\delta}_{a2}(t)$, $\underline{\delta}_{b2}(t)$ are prescribed performance functions, which are used to restrict the upper and lower bounds of z_1 .

Similar to Equation (3.2), the time derivation of Equation (3.9) is

$$\dot{V}_2 = \xi_2 z_1 \dot{z}_1 + \varpi_2 z_1^2 \tag{3.10}$$

where the expressions of ξ_2 and ϖ_2 are

$$\begin{cases} \xi_2 = 1 + \frac{q(z_1)}{\bar{\delta}_{a2}^2 - z_1^2} + \frac{1 - q(z_1)}{\underline{\delta}_{b2}^2 - z_1^2} \\ \varpi_2 = - \left(\frac{q(z_1) \dot{\bar{\delta}}_{a2}}{\bar{\delta}_{a2} (\bar{\delta}_{a2}^2 - z_1^2)} + \frac{(1 - q(z_1)) \dot{\underline{\delta}}_{b2}}{\underline{\delta}_{b2} (\underline{\delta}_{b2}^2 - z_1^2)} \right) \end{cases} \tag{3.11}$$

The designed virtual control law is α used to stabilise z_1 :

$$\alpha = - \left(k_1 + \frac{\xi_2}{2} + \frac{\varpi_2}{\xi_2} \right) z_1 + \dot{\psi}_d - \dot{\lambda}_1 \tag{3.12}$$

where $k_1 > 0$.

To avoid derivation of the virtual control law α , we introduce the dynamic surface control. Let α pass the following first-order low-pass filter:

$$\begin{cases} T\dot{r}_d + r_d = \alpha \\ r_d(0) = \alpha(0) \end{cases} \tag{3.13a}$$

$$y_1 = r_d - \alpha \tag{3.13b}$$

where r_d is the state variable of the first-order low-pass filter, T is the filter time constant and y_1 is the filter output error.

According to Equations (3.6)–(3.13) and the Young’s inequality, \dot{V}_2 can be further written as

$$\begin{aligned} \dot{V}_2 &= \xi_2 z_1 z_2 - \frac{\xi_2^2}{2} z_1^2 + \xi_2 z_1 y_1 - k_1 \xi_2 z_1^2 \\ &\leq \xi_2 z_1 z_2 - k_1 \xi_2 z_1^2 + \frac{1}{2} y_1^2 \end{aligned} \tag{3.14}$$

Step 2: According to Equations (2.3) and (3.7), the time derivation of z_2 is

$$\begin{aligned} \dot{z}_2 = & \frac{1}{m_{33}}((m_{11} - m_{22})uv - d_{33}r - \Delta f_r \\ & + d_r + t_r - m_{33}\dot{r}_d + \hat{h}_2 m_{33} \lambda_2) \end{aligned} \tag{3.15}$$

Consider that there are model uncertainties $\Delta f = [\Delta f_u, \Delta f_v, \Delta f_r]^T$ in the three-degrees-of-freedom surface vessel. According to the universal approximation characteristics of the RBF neural network, we first approximate Δf_r , where the output expression is given as

$$\Delta f_r = \mathbf{W}_r^* \mathbf{h}(\mathbf{z}) + e_{wr}(\mathbf{z}) \tag{3.16}$$

where $\mathbf{z} = [u, v, r]^T$ is the input vector of the neural network.

Here, $\mathbf{h}(\mathbf{z}) = [h_1(z), h_2(z), \dots, h_n(z)]^T$ is the vector of radial basis function. The specific expression is given by

$$h_j(z) = \exp \left[-\frac{\|\mathbf{z} - \mathbf{c}_j\|^2}{2b_j^2} \right], \quad (j = 1, \dots, n) \tag{3.17}$$

where $b_j > 0$ is the width of the Gaussian function; $\mathbf{c}_j = [c_1, c_2, \dots, c_m]^T \in \mathbf{R}^m$ is the centre of the Gaussian function, which has the same dimension as the input vector \mathbf{z} ; $e_{wr}(\mathbf{z})$ is the approximation error of neural network; and $\mathbf{W}_r^* = [w_{r,1}^*, w_{r,2}^*, \dots, w_{r,n}^*]^T \in \mathbf{R}^{n \times 1}$ is the ideal weight vector, that is, the value of the vector \mathbf{W}_r^* which makes $|e_{wr}(\mathbf{z})|$ the smallest for all $\mathbf{z} \in \Omega_z$. Here, \mathbf{W}_r^* is given by

$$\mathbf{W}_r^* = \arg \min_{\mathbf{W} \in \mathbf{R}^n} \left\{ \sup_{\mathbf{z} \in \Omega} |\Delta f_r(\mathbf{z}) - \mathbf{W}_r^T \mathbf{h}(\mathbf{z})| \right\} \tag{3.18}$$

In practical applications, the ideal weight vector \mathbf{W}_r^* cannot be obtained, so the estimation $\hat{\mathbf{W}}_r$ of \mathbf{W}_r^* needs to be used in the controller design, and $\tilde{\mathbf{W}}_r = \hat{\mathbf{W}}_r - \mathbf{W}_r^*$.

Assumption 6. For all $\mathbf{z} \in \Omega_z$, the ideal weight vector \mathbf{W}_r^* of the neural network and the approximation error $e_{wr}(\mathbf{z})$ are bounded, that is, there are positive constants $\mathbf{W}_{r,\max}$ and bounded functions $e_{wr,\max}(\mathbf{z})$ that satisfy $\|\mathbf{W}_r^*\| \leq \mathbf{W}_{r,\max}$ and $e_{wr}(\mathbf{z}) \leq e_{wr,\max}(\mathbf{z})$. By Assumption 1, path following external environmental disturbance d_r and approximation error $e_{wr}(\mathbf{z})$, there is a bounded function $\lambda_r > 0$, which makes $|e_{wr}(\mathbf{z})| + |d_r| < \lambda_r$

Remark 8. To simplify the description, in this paper, the neural network approximation error $e_{wr}(\mathbf{z})$ and environmental disturbance d_r are collectively referred to as compound disturbance, where λ_r is the bounding of compound disturbance.

Then, we design the control input t_r as

$$\begin{aligned} t_r = & -(m_{11} - m_{22})uv + d_{33}r - c_2 m_{33} \lambda_2 - k_2 z_2 \\ & - \left(1 + \frac{q(z_1)}{\delta_{a2}^2 - z_1^2} + \frac{1 - q(z_1)}{\delta_{b2}^2 - z_1^2} \right) z_1 + m_{33} \dot{r}_d + \hat{\mathbf{W}}_r^T \mathbf{h}(\mathbf{z}) - \hat{\lambda}_r \phi(z_2) \end{aligned} \tag{3.19}$$

where $\gamma_1 > 0$ and $\sigma_1 > 0$ are the design constants, $\phi(z_2) = \tanh(z_2/\varepsilon_1)$, $\varepsilon_1 > 0$ is the design constants and $\hat{\lambda}_r^0$ is the prior estimate of $\hat{\lambda}_r$.

The weight update law and the adaptive law of the estimation $\hat{\lambda}_r$ are designed as

$$\dot{\hat{\mathbf{W}}}_r = -\Gamma_1 [z_2 \mathbf{h}(\mathbf{z}) + \vartheta_1 \hat{\mathbf{W}}_r] \tag{3.20a}$$

$$\dot{\hat{\lambda}}_r = \gamma_1 [z_2 \phi(z_2) - \sigma_1 (\hat{\lambda}_r - \hat{\lambda}_r^0)] \tag{3.20b}$$

Table 1. Model parameters of surface vessel simulation.

Parameter	Value	Parameter	Value
M_{11}	$5 \cdot 3122 \times 10^6$	C_{31}	$8 \cdot 2831 \times 10^6 v$
M_{12}	$8 \cdot 2831 \times 10^6$	C_{32}	$-5 \cdot 3122 \times 10^6 u$
M_{13}	$3745 \cdot 4 \times 10^6$	D_{11}	$5 \cdot 0242 \times 10^4$
C_{13}	$-8 \cdot 2831 \times 10^6 v$	D_{12}	$27 \cdot 229 \times 10^4$
C_{23}	$5 \cdot 3122 \times 10^6 u$	D_{13}	41894×10^4

Table 2. Control parameters of surface vessel simulation.

Parameter	Value	Parameter	Value	Parameter	Value
\tilde{h}_1	100	Γ_1	1×10^4	σ_2	1×10^{-7}
\tilde{h}_2	100	Γ_2	1×10^5	σ_3	1×10^{-9}
\tilde{h}_3	10	Γ_3	1×10^5	ε_1	1×10^{-9}
\tilde{h}_4	10	ϑ_1	1×10^{-6}	ε_2	1×10^{-9}
k_Δ	0.01	ϑ_2	1×10^{-4}	ε_3	1
k_θ	1	ϑ_3	1×10^{-4}	$\hat{\lambda}_u^0$	0.1
k_1	0.001	γ_1	1×10^5	$\hat{\lambda}_v^0$	0.1
k_2	10	γ_2	5×10^4	$\hat{\lambda}_r^0$	0.1
k_3	10	γ_3	5×10^4	T	0.01
k_4	10	σ_1	5×10^{-7}		

Table 3. Prescribed performance functions of surface vessel simulation.

Constrained error	Prescribed performance function
x_e	$\begin{cases} \bar{\delta}_{a1}(t) = (1500 - 10)e^{-0.2t} + 10 \\ \underline{\delta}_{b1}(t) = (1200 - 8)e^{-0.2t} + 8 \end{cases}$
y_e	$\begin{cases} \bar{\delta}_{c1}(t) = (800 - 10)e^{-1.75t} + 10 \\ \underline{\delta}_{d1}(t) = (600 - 8)e^{-1.75t} + 8 \end{cases}$
ψ_e	$\begin{cases} \bar{\delta}_{a2}(t) = (0.8 - 0.1)e^{-0.1t} + 0.1 \\ \underline{\delta}_{b2}(t) = (0.7 - 0.08)e^{-0.1t} + 0.08 \end{cases}$

where $\gamma_1 > 0$ and $\sigma_1 > 0$ are the design constants, $\phi(z_2) = \tanh(z_2/\varepsilon_1)$, $\varepsilon_1 > 0$ are the design constants and $\hat{\lambda}_r^0$ is the prior estimate of $\hat{\lambda}_r$.

Remark 9. For the design of control input t_r at this stage, the neural network and the adaptive law only approximate the model uncertainties Δf_r and disturbances d_r . In the next design of control input t_u and t_v , $(\Delta f_u, \Delta f_v)$ and (d_u, d_v) will be estimated, the specific process is similar.

3.3. Velocity tracking control

To compensate for saturation of controller inputs τ_u and τ_v , two first-order adaptive assistant systems

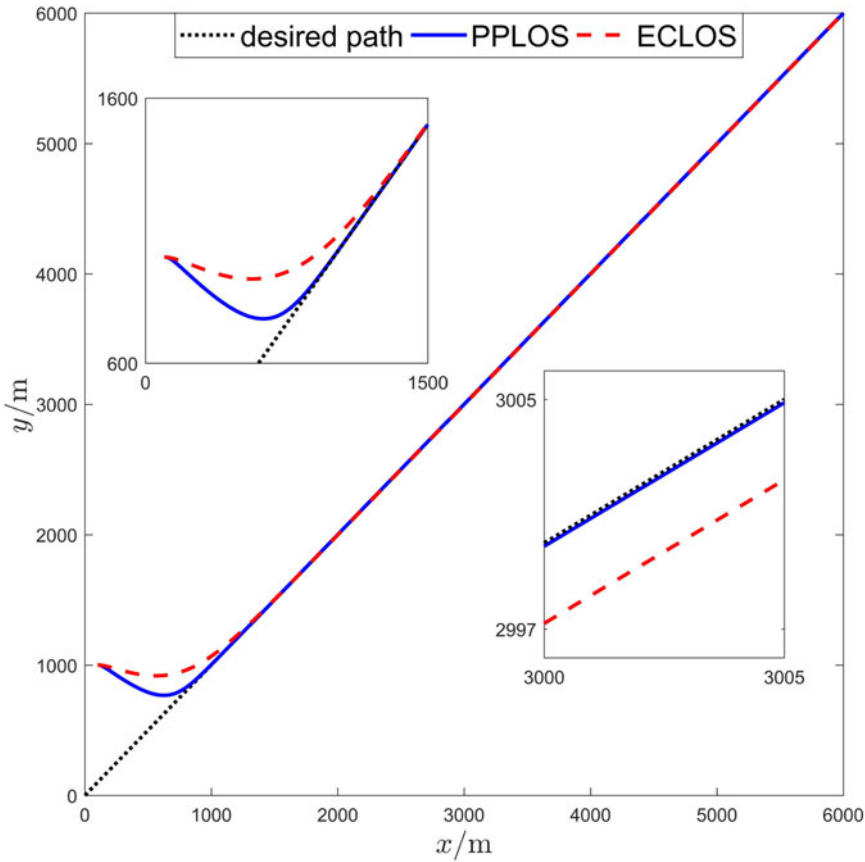


Figure 5. Straight line path following.

are introduced as

$$\begin{bmatrix} \dot{\lambda}_3 \\ \dot{\lambda}_4 \end{bmatrix} = \begin{bmatrix} -\tilde{h}_3\lambda_3 + \frac{1}{m_{11}}\Delta t_u \\ -\tilde{h}_4\lambda_4 + \frac{1}{m_{22}}\Delta t_v \end{bmatrix} \tag{3.21}$$

The surface vessel’s surge error z_1 and sway error z_2 can be obtained as

$$\begin{bmatrix} z_3 \\ z_4 \end{bmatrix} = \begin{bmatrix} u - u_d - \lambda_3 \\ v - v_d - \lambda_4 \end{bmatrix} \tag{3.22}$$

Remark 10. Since the research object of this paper is a fully actuated surface vessel with three controller inputs, which is different from an underactuated surface vessel, we cannot only control the surge, but can also control the sway of the surface vessel.

According to Equations (2.3) and (3.22), we can find the time derivative of z_3 and z_4 as

$$\begin{bmatrix} \dot{z}_3 \\ \dot{z}_4 \end{bmatrix} = \begin{bmatrix} \frac{1}{m_{11}}(m_{22}vr - d_{11}u - \Delta f_u) + \frac{sat_u(\tau_u) + d_u}{m_{11}} - \dot{u}_d - \dot{\lambda}_3 \\ \frac{1}{m_{22}}(-m_{11}ur - d_{22}v - \Delta f_v) + \frac{sat_v(\tau_v) + d_v}{m_{22}} - \dot{v}_d - \dot{\lambda}_4 \end{bmatrix} \tag{3.23}$$

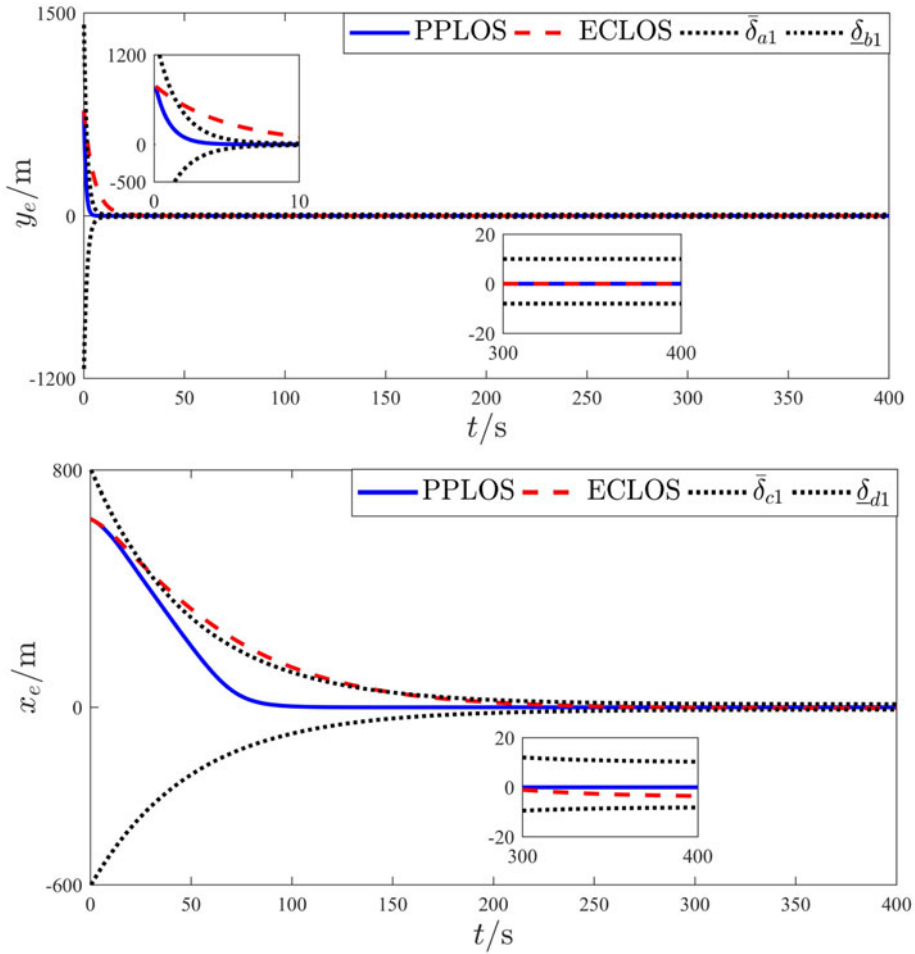


Figure 6. Position errors of straight line path following.

Similarly, two neural networks are designed to approximate the model uncertainties Δf_u and Δf_v , and the output expression of the neural network is

$$\begin{cases} \Delta f_u = \mathbf{W}_u^* \mathbf{h}(\mathbf{z}) + e_{w_u}(\mathbf{z}) \\ \Delta f_v = \mathbf{W}_v^* \mathbf{h}(\mathbf{z}) + e_{w_v}(\mathbf{z}) \end{cases} \quad (3.24)$$

Let $\hat{\mathbf{W}}_u$ be the estimated value of \mathbf{W}_u^* and $\hat{\mathbf{W}}_v$ be the estimated value of \mathbf{W}_v^* . We design the control input t_u and t_v as

$$\begin{cases} \tau_u = -k_3 z_3 + m_{11} \dot{u}_d - \hat{h}_3 m_{11} \lambda_3 - m_{22} v r + d_{11} u + \hat{\mathbf{W}}_u^T \mathbf{h}(\mathbf{z}) - \hat{\lambda}_u \phi(z_3) \\ \tau_v = -k_4 z_4 + m_{22} \dot{v}_d - \hat{h}_4 m_{22} \lambda_4 + m_{11} u r + d_{22} v + \hat{\mathbf{W}}_v^T \mathbf{h}(\mathbf{z}) - \hat{\lambda}_v \phi(z_4) \end{cases} \quad (3.25)$$

We design the weight update law and the adaptive law of the estimation as

$$\begin{cases} \dot{\hat{\mathbf{W}}}_u = -\Gamma_2 [z_2 \mathbf{h}(\mathbf{z}) + \vartheta_2 \hat{\mathbf{W}}_u] \\ \dot{\hat{\mathbf{W}}}_v = -\Gamma_3 [z_3 \mathbf{h}(\mathbf{z}) + \vartheta_3 \hat{\mathbf{W}}_v] \end{cases} \quad (3.26a)$$

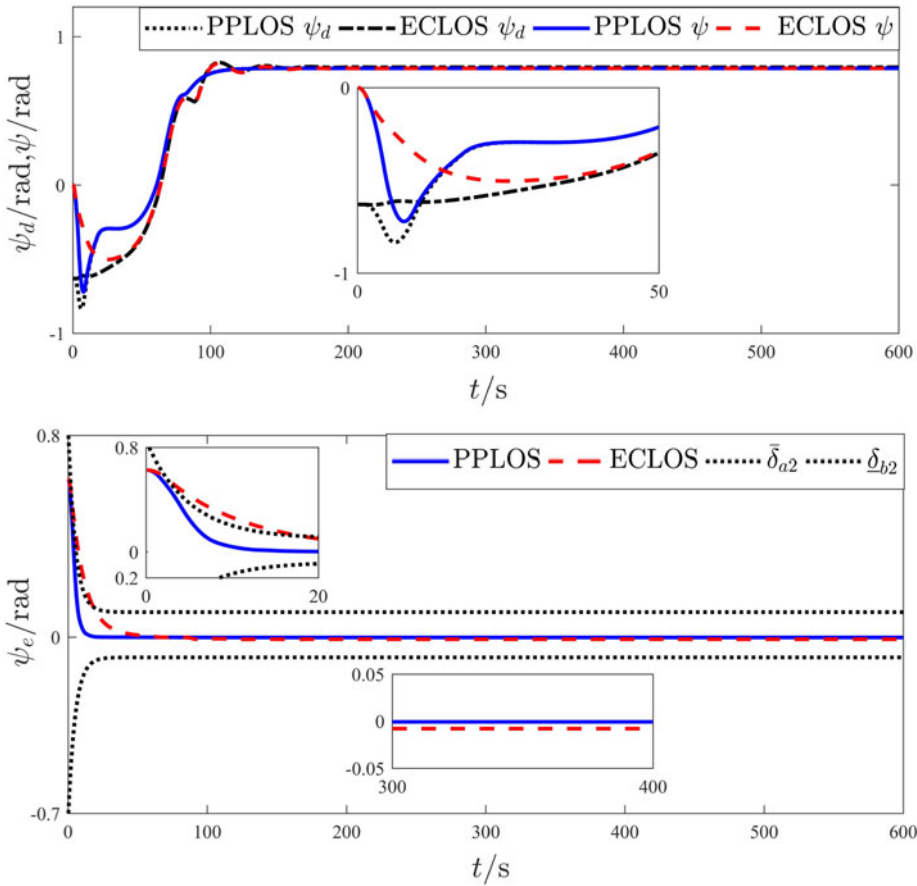


Figure 7. Desired heading angle, heading angle and heading errors of straight line path following.

$$\begin{cases} \dot{\hat{\lambda}}_u = \gamma_2 [z_3 \phi(z_3) - \sigma_2 (\hat{\lambda}_u^* - \lambda_u^0)] \\ \dot{\hat{\lambda}}_v = \gamma_3 [z_4 \phi(z_4) - \sigma_3 (\hat{\lambda}_v^* - \lambda_v^0)] \end{cases} \quad (3.26b)$$

where $\Gamma_2 > 0$, $\Gamma_3 > 0$, $\vartheta_2 > 0$, $\vartheta_3 > 0$, $\gamma_2 > 0$, $\gamma_3 > 0$, $\sigma_2 > 0$, $\sigma_3 > 0$ and $\phi(z_3) = \tanh(z_3/\varepsilon_2)$, $\phi(z_4) = \tanh(z_4/\varepsilon_3)$, $\varepsilon_2 > 0$, $\varepsilon_3 > 0$ are the design constants. The bounds λ_u and λ_v of the compound disturbance satisfy $|e_{wu}(z)| + |d_u| < \lambda_u$, $|e_{wv}(z)| + |d_v| < \lambda_v$, where λ_u^0 is the prior estimate of $\hat{\lambda}_u$ and λ_v^0 is the prior estimate of $\hat{\lambda}_v$.

4. Stability analysis

Consider the candidate Lyapunov function as

$$\begin{aligned} V = & V_1 + m_{33}V_2 + \frac{1}{2}m_{33}z_2^2 + \frac{1}{2}m_{11}z_3^2 + \frac{1}{2}m_{22}z_4^2 + \frac{1}{2}y^2 \\ & + \frac{1}{2\gamma_2}\tilde{\lambda}_r^2 + \frac{1}{2\gamma_1}\tilde{\lambda}_u^2 + \frac{1}{2\gamma_2}\tilde{\lambda}_v^2 \\ & + \frac{1}{2\Gamma_3}\tilde{W}_r^T\tilde{W}_r + \frac{1}{2\Gamma_1}\tilde{W}_u^T\tilde{W}_u + \frac{1}{2\Gamma_2}\tilde{W}_v^T\tilde{W}_v \end{aligned} \quad (4.1)$$

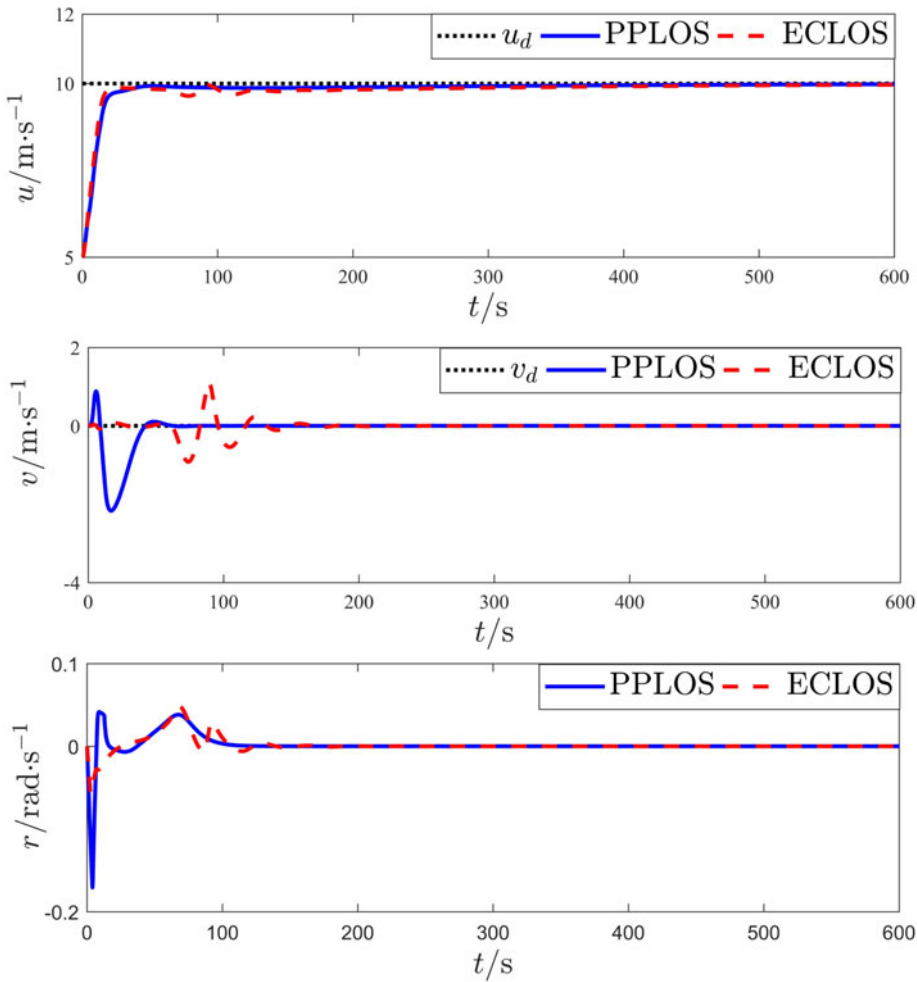


Figure 8. Actual velocity of straight line path following.

where $\tilde{W}_u = \hat{W}_u - W_u^*$, $\tilde{W}_v = \hat{W}_v - W_v^*$ and $\tilde{W}_r = \hat{W}_r - W_r^*$ are the weight approximation errors of three neural networks. Here, $\tilde{\lambda}_u = \lambda_u - \hat{\lambda}_u$, $\tilde{\lambda}_v = \lambda_v - \hat{\lambda}_v$ and $\tilde{\lambda}_r = \lambda_r - \hat{\lambda}_r$ are the estimation errors.

In light of Equations (3.3)–(3.5), (3.14)–(3.17), (3.19)–(3.20) and (3.23)–(3.26), the time derivation of V is

$$\begin{aligned} \dot{V} &= \dot{V}_1 + \dot{V}_2 + m_{33}z_2\dot{z}_2 + m_{11}z_3\dot{z}_3 + m_{22}z_4\dot{z}_4 + y_1\dot{y}_1 - \frac{1}{\gamma_1}\tilde{\lambda}_r\dot{\lambda}_r \\ &\quad - \frac{1}{\gamma_2}\tilde{\lambda}_u\dot{\lambda}_u - \frac{1}{\gamma_3}\tilde{\lambda}_v\dot{\lambda}_v + \frac{1}{\Gamma_1}\tilde{W}_r^T\dot{W}_r + \frac{1}{\Gamma_2}\tilde{W}_u^T\dot{W}_u + \frac{1}{\Gamma_3}\tilde{W}_v^T\dot{W}_v \\ &= \dot{V}_1 + \dot{V}_2 - k_2z_2^2 - \xi_1z_1z_2 + z_2(\tilde{W}_r^T\mathbf{h}(z) - \tilde{\lambda}_r\phi(z_2) - e_{wr}(z) + d_r) \\ &\quad - k_3z_3^2 + z_3(\tilde{W}_u^T\mathbf{h}(z) - \tilde{\lambda}_u\phi(z_3) - e_{wu}(z) + d_u) - k_4z_4^2 \\ &\quad + z_4(\tilde{W}_v^T\mathbf{h}(z) - \tilde{\lambda}_v\phi(z_4) - e_{wv}(z) + d_v) - \tilde{\lambda}_r(z_2\phi(z_2) - \sigma_1(\tilde{\lambda}_r - \lambda_r^0)) \\ &\quad - \tilde{\lambda}_u(z_3\phi(z_3) - \sigma_2(\tilde{\lambda}_u - \lambda_u^0)) - \tilde{\lambda}_v(z_4\phi(z_4) - \sigma_3(\tilde{\lambda}_v - \lambda_v^0)) \\ &\quad - \tilde{W}_r^Tz_2\mathbf{h}(z) - \tilde{W}_u^Tz_3\mathbf{h}(z) - \tilde{W}_v^Tz_4\mathbf{h}(z) - \vartheta_1\tilde{W}_r^T\hat{W}_r \end{aligned}$$

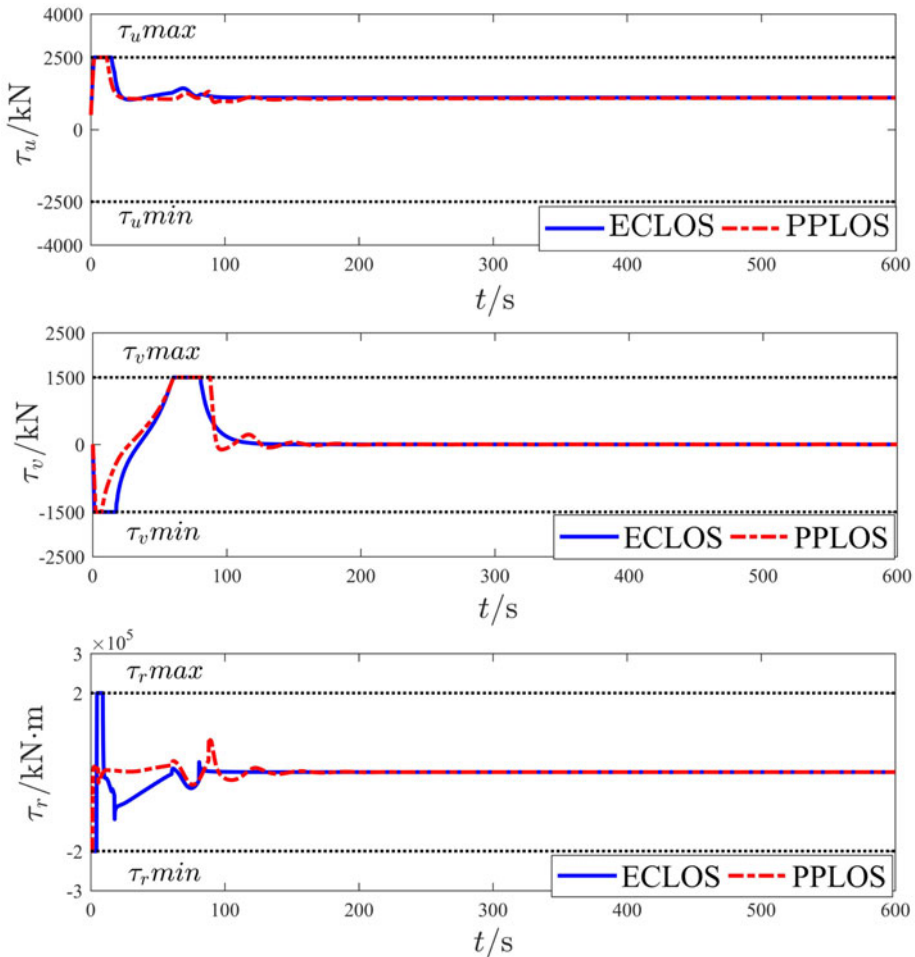


Figure 9. Input signal of straight line path following.

$$\begin{aligned}
 & -\partial_2 \tilde{W}_u^T \hat{W}_u - \partial_3 \tilde{W}_v^T \hat{W}_v + y_1 \dot{y}_1 & (4.2a) \\
 \leq & -k_\theta \xi_{11} x_e^2 - \frac{k_\Delta \xi_{12} U}{\sqrt{1 + (k_\Delta y_e)^2}} y_e^2 - k_1 \xi_2 z_1^2 - k_2 z_2^2 - k_3 z_3^2 - k_4 z_4^2 \\
 & + \lambda_r (|z_2| - z_2 \phi(z_2)) + \lambda_u (|z_3| - z_3 \phi(z_3)) + \lambda_v (|z_4| - z_4 \phi(z_4)) \\
 & - z_2 e_{wr} - z_3 e_{wu} - z_4 e_{wv} - \sigma_1 (\hat{t}_r - \lambda_r) (\hat{t}_r - \lambda_r^0) - \sigma_2 (\hat{t}_u - \lambda_u) (\hat{t}_u - \lambda_u^0) \\
 & - \sigma_3 (\hat{t}_v - \lambda_v) (\hat{t}_v - \lambda_v^0) - \partial_1 \tilde{W}_r^T \hat{W}_r - \partial_2 \tilde{W}_u^T \hat{W}_u - \partial_3 \tilde{W}_v^T \hat{W}_v \\
 & + y_1 \dot{y}_1 + \frac{1}{2} y_1^2 & (4.2b)
 \end{aligned}$$

According to the nature of the hyperbolic tangent function, for any $\varepsilon > 0$, $\iota \in \mathbb{R}$, $0 \leq |\iota| - \iota \phi(\iota) = |\iota| - \tanh(\iota/\varepsilon) \leq 0.2785\varepsilon$, we have

$$\begin{cases} |z_2| - z_2 \phi(z_2) = |z_2| - \tanh(z_2/\varepsilon_1) \leq 0.2785\varepsilon_1 \\ |z_3| - z_3 \phi(z_3) = |z_3| - \tanh(z_3/\varepsilon_2) \leq 0.2785\varepsilon_2 \\ |z_4| - z_4 \phi(z_4) = |z_4| - \tanh(z_4/\varepsilon_3) \leq 0.2785\varepsilon_3 \end{cases} \quad (4.3)$$

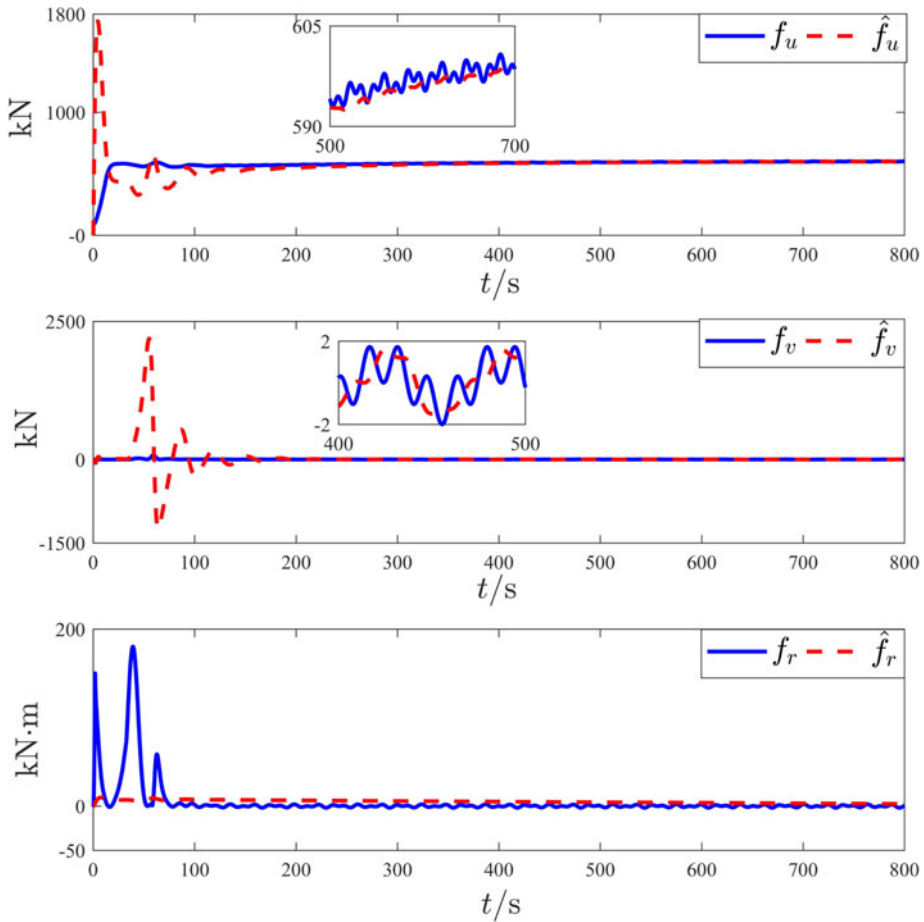


Figure 10. Approximation curves of model uncertainties of straight line path following.

and consider the following inequalities:

$$\begin{cases} -e_{wr}z_2 \leq \frac{e_{wr}^2}{2} + \frac{z_2^2}{2} \leq \frac{e_{wr,max}^2}{2} + \frac{z_2^2}{2} \\ -e_{wu}z_3 \leq \frac{e_{wu}^2}{2} + \frac{z_3^2}{2} \leq \frac{e_{wu,max}^2}{2} + \frac{z_3^2}{2} \\ -e_{wv}z_4 \leq \frac{e_{wv}^2}{2} + \frac{z_4^2}{2} \leq \frac{e_{wv,max}^2}{2} + \frac{z_4^2}{2} \end{cases} \quad (4.4a)$$

$$\begin{cases} -\vartheta_1 \tilde{W}_r^T \hat{W}_r \leq -\frac{\vartheta_1}{2} \tilde{W}_r^T \tilde{W}_r + \frac{\vartheta_1}{2} W_{r,max}^2 \\ -\vartheta_2 \tilde{W}_u^T \hat{W}_u \leq -\frac{\vartheta_2}{2} \tilde{W}_u^T \tilde{W}_u + \frac{\vartheta_2}{2} W_{u,max}^2 \\ -\vartheta_3 \tilde{W}_v^T \hat{W}_v \leq -\frac{\vartheta_3}{2} \tilde{W}_v^T \tilde{W}_v + \frac{\vartheta_3}{2} W_{v,max}^2 \end{cases} \quad (4.4b)$$

$$\begin{aligned} & -(\hat{\lambda}_i - \lambda_i)(\hat{\lambda}_i - \lambda_i^0) = -\frac{1}{2}(\hat{\lambda}_i - \lambda_i)^2 - \frac{1}{2}(\hat{\lambda}_i - \lambda_i^0)^2 + \frac{1}{2}(\lambda_i - \lambda_i^0)^2 \\ & \leq -\frac{1}{2}\hat{\lambda}_i^2 + \frac{1}{2}(\lambda_i - \lambda_i^0)^2, \quad (i = u, v, r) \end{aligned} \quad (4.4c)$$

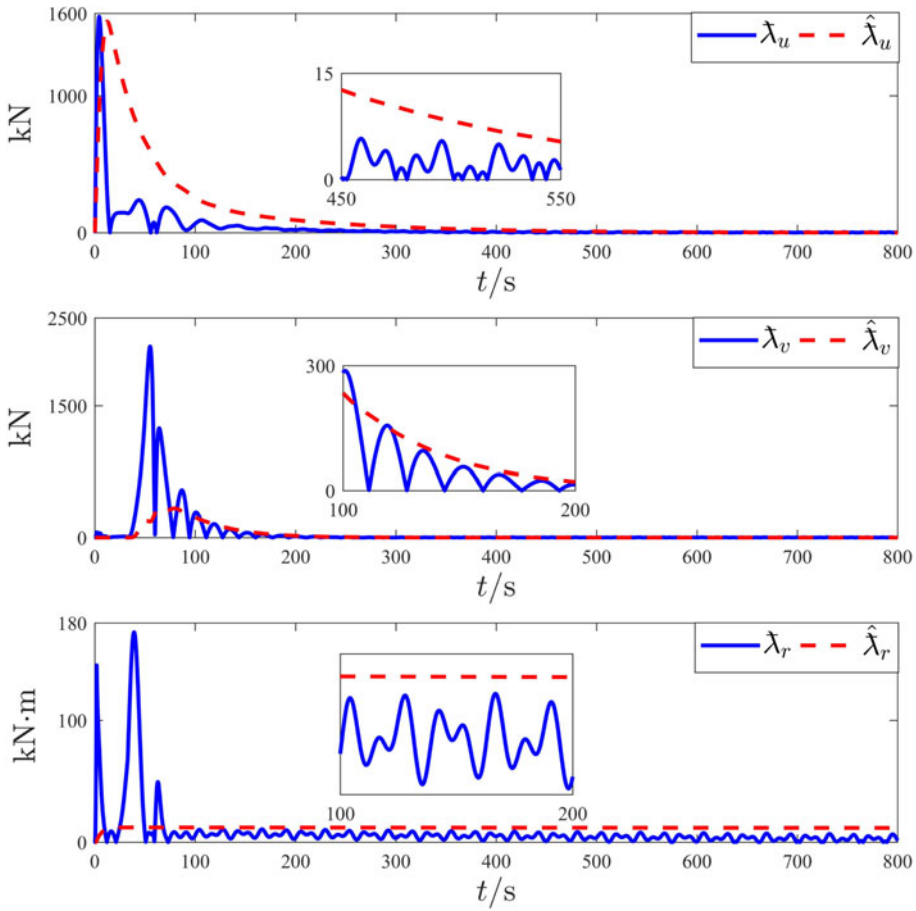


Figure 11. Curves of the bounds of the compound disturbances and its estimation.

According to Equation (3.13), the time derivation of y_1 is

$$\begin{aligned} \dot{y}_1 &= \dot{r}_d - \dot{\alpha} = -y_1/T - \dot{\alpha} \\ &= -y_1/T - \zeta_\alpha(z_1, \dot{z}_1, \dot{\psi}_d, \dot{\psi}_d, y_1, \lambda_1, \dot{\lambda}_1 \dots) \end{aligned} \tag{4.5}$$

For $B_0 > 0, \Theta_0 > 0$, consider the following compact sets:

$$\begin{aligned} \Omega_d &= \{(x_d, \dot{x}_d, \ddot{x}_d, y_d, \dot{y}_d, \ddot{y}_d, u_d, \dot{u}_d, \ddot{u}_d, v_d, \dot{v}_d, \ddot{v}_d) : \\ &\quad x_d^2 + \dot{x}_d^2 + \ddot{x}_d^2 + y_d^2 + \dot{y}_d^2 + \ddot{y}_d^2 \\ &\quad + u_d^2 + \dot{u}_d^2 + \ddot{u}_d^2 + v_d^2 + \dot{v}_d^2 + \ddot{v}_d^2 \leq B_0\} \end{aligned} \tag{4.6a}$$

$$\Omega_1 = \{(x_e, y_e, z_1, z_2, z_3, z_4, y_1, \tilde{\lambda}_r, \tilde{\lambda}_u, \tilde{\lambda}_v, \tilde{W}_r, \tilde{W}_u, \tilde{W}_v) : L_1 \leq \Theta_0\} \tag{4.6b}$$

where $\Omega_d \times \Omega_1$ is also compact set, and the nonlinear continuous function $\zeta_\alpha(\cdot)$ has the maximum value N_u on the compact set $\Omega_d \times \Omega_1$.

Table 4. Prescribed performance functions of surface vessel simulation.

Constrained error	Prescribed performance function
x_e	$\begin{cases} \bar{\delta}_{a1}(t) = (1500 - 10)e^{-0.2t} + 10 \\ \underline{\delta}_{b1}(t) = (1200 - 8)e^{-0.2t} + 8 \end{cases}$
y_e	$\begin{cases} \bar{\delta}_{c1}(t) = (800 - 20)e^{-1.75t} + 20 \\ \underline{\delta}_{d1}(t) = (600 - 16)e^{-1.75t} + 16 \end{cases}$
ψ_e	$\begin{cases} \bar{\delta}_{a2}(t) = (1.2 - 0.1)e^{-0.1t} + 0.1 \\ \underline{\delta}_{b2}(t) = (1 - 0.08)e^{-0.1t} + 0.08 \end{cases}$

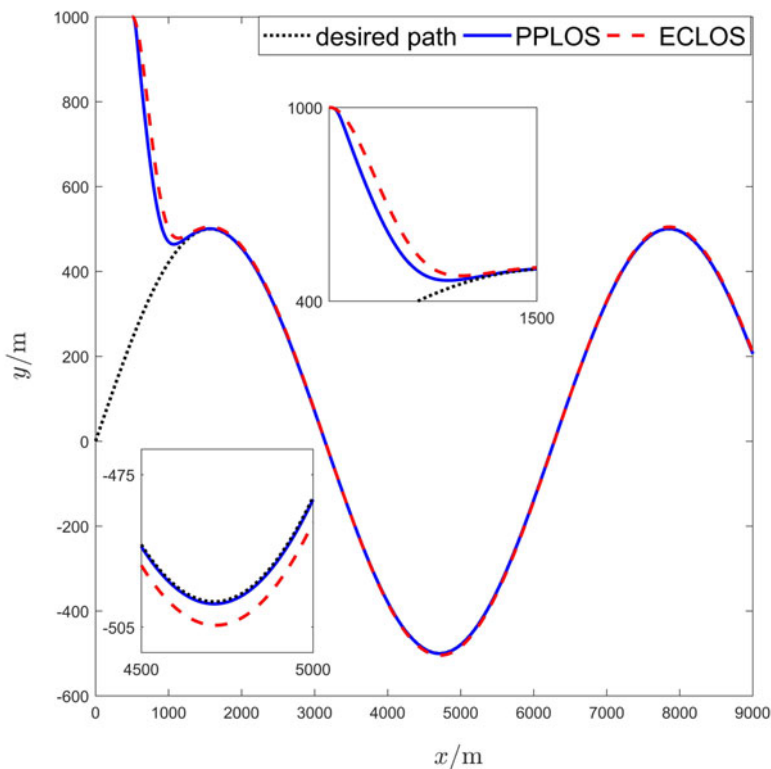


Figure 12. Sin curve path following.

In light of Equations (4.5) and (4.6), we can get

$$\begin{aligned} y_1 \dot{y}_1 &= -\frac{y_1^2}{T} + \frac{y_1^2}{T} + y_1 \dot{y}_1 = -\frac{y_1^2}{T} + y_1 \left(\frac{y_1}{T} + \dot{y}_1 \right) \\ &\leq -\frac{y_1^2}{T} + \alpha_1 y_1^2 + \frac{N_u^2}{4\alpha_1} \end{aligned} \tag{4.7}$$

where α_1 is the design constant.

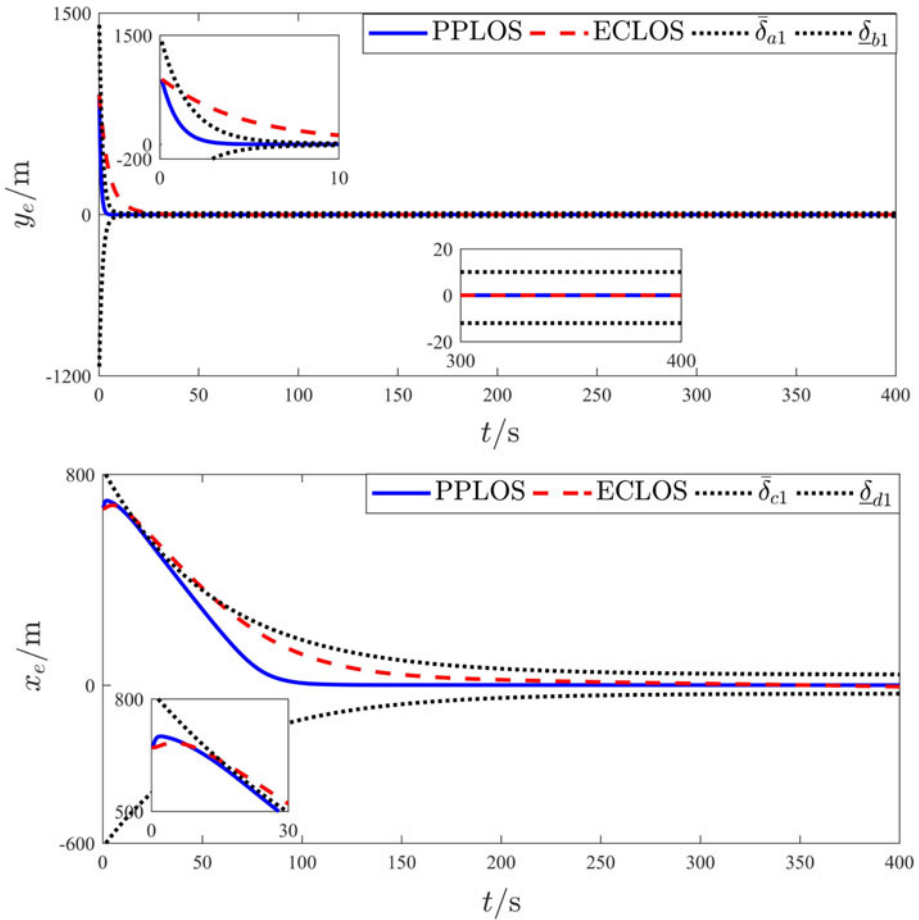


Figure 13. Position errors of sin curve path following.

According to Equations (4.3), (4.4) and (4.7), \dot{V} can be written as

$$\begin{aligned} \dot{V} \leq & -k_\theta \xi_{11} x_e^2 - \frac{k_\Delta \xi_{12} U}{\sqrt{1 + (k_\Delta y_e)^2}} y_e^2 - k_1 \xi_{22} z_1^2 \\ & - \frac{2k_2 - 1}{2} z_2^2 - \frac{2k_3 - 1}{2} z_3^2 - \frac{2k_4 - 1}{2} z_4^2 \\ & - \frac{\sigma_1}{2} \tilde{\tau}_r^2 - \frac{\sigma_2}{2} \tilde{\tau}_u^2 - \frac{\sigma_3}{2} \tilde{\tau}_v^2 - \frac{\vartheta_1}{2} \tilde{\mathbf{W}}_r^T \tilde{\mathbf{W}} \\ & - \frac{\vartheta_2}{2} \tilde{\mathbf{W}}_u^T \tilde{\mathbf{W}}_u - \frac{\vartheta_3}{2} \tilde{\mathbf{W}}_v^T \tilde{\mathbf{W}}_v - \left(\frac{1}{T} - \alpha_1 - \frac{1}{2} \right) y_1^2 \\ & + 0 \cdot 2785 z_2 \tilde{\tau}_r + 0 \cdot 2785 z_3 \tilde{\tau}_u + 0 \cdot 2785 z_4 \tilde{\tau}_v \\ & + \frac{e_{r,\max}^2}{2} + \frac{e_{u,\max}^2}{2} + \frac{e_{v,\max}^2}{2} + \frac{\sigma_1}{2} (\tilde{\tau}_r - \tilde{\tau}_r^0)^2 \end{aligned}$$

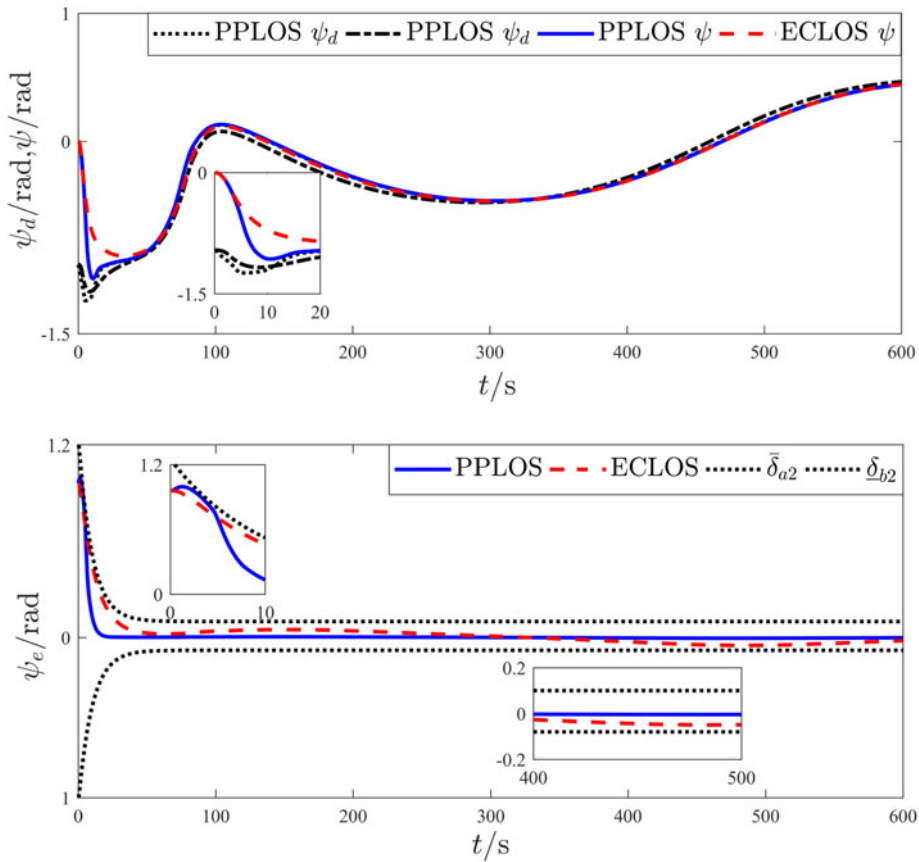


Figure 14. Desired heading angle, heading angle and heading errors of sin curve path following.

$$\begin{aligned}
 & + \frac{\sigma_2}{2} (\bar{\lambda}_u - \lambda_u^0)^2 + \frac{\sigma_3}{2} (\bar{\lambda}_r - \lambda_r^0)^2 + \frac{\vartheta_1}{2} \mathbf{W}_r^2 \\
 & + \frac{\vartheta_2}{2} \mathbf{W}_u^2 + \frac{\vartheta_3}{2} \mathbf{W}_v^2 + \frac{N_u^2}{4\alpha_1}
 \end{aligned} \tag{4.8}$$

According to Theorem 1, Equation (4.7) can be rewritten as

$$\dot{V} \leq -\mu_1 V + C_1 \tag{4.9}$$

where

$$\begin{aligned}
 \mu_1 = \min \left\{ & 2k_\theta, 2k_\Delta U / \sqrt{1 + (k_\Delta y_e)^2}, \right. \\
 & 2k_1 z_1^2, (1 - 2k_2), (1 - 2k_3), \\
 & (1 - 2k_4), \sigma_1, \sigma_2, \sigma_3, \vartheta_1, \vartheta_2, \\
 & \left. \vartheta_3, 2 \left(\frac{1}{T} - \alpha_1 - \frac{1}{2} \right) \right\} > 0 \tag{4.10a}
 \end{aligned}$$

$$\begin{aligned}
 C_1 = & 0 \cdot 2785z_2\bar{\lambda}_r + 0 \cdot 2785z_3\bar{\lambda}_u + 0 \cdot 2785z_4\bar{\lambda}_v \\
 & + \frac{e_{r,\max}^2}{2} + \frac{e_{u,\max}^2}{2} + \frac{e_{v,\max}^2}{2} + \frac{\sigma_1}{2} (\bar{\lambda}_r - \lambda_r^0)^2
 \end{aligned}$$

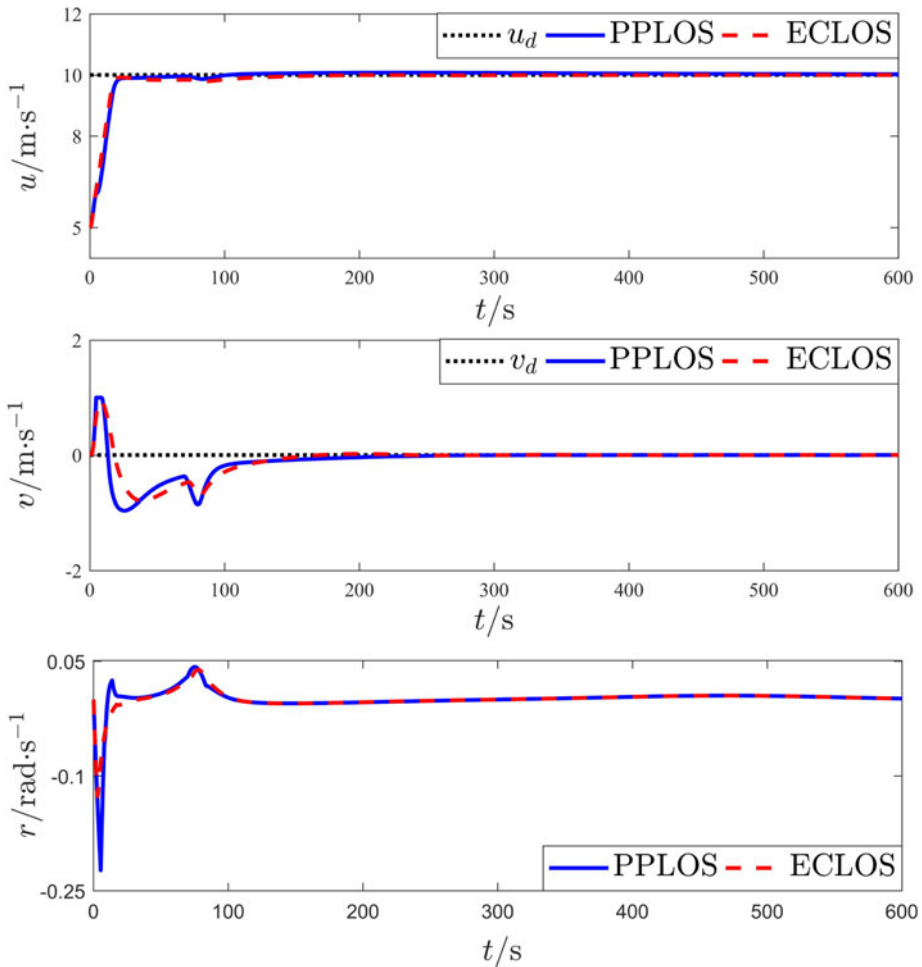


Figure 15. Actual velocity of sin curve path following.

$$\begin{aligned}
 & + \frac{\sigma_2}{2} (\tilde{x}_u - \tilde{x}_u^0)^2 + \frac{\sigma_3}{2} (\tilde{x}_v - \tilde{x}_v^0) + \frac{\vartheta_1}{2} W_r^2 \\
 & + \frac{\vartheta_2}{2} W_u^2 + \frac{\vartheta_3}{2} W_v^2 + \frac{N_u^2}{4\alpha_1}
 \end{aligned} \tag{4.10b}$$

Hence, we can get

$$0 \leq V(t) \leq \frac{C_1}{\mu_1} + \left[V(0) - \frac{C_1}{\mu_1} \right] e^{-\mu_1 t} \tag{4.11}$$

Since $\lim_{t \rightarrow \infty} V(t) = C_1/V_1$, we know $V(t)$ is uniformly ultimately bounded. From Equation (49), the signal $x_e, y_e, z_1, z_2, z_3, z_4, y_1, \tilde{\lambda}_r, \tilde{\lambda}_u, \tilde{\lambda}_v, \tilde{W}_r, \tilde{W}_u, \tilde{W}_v$ is consistent and finally bounded. From the boundedness of x_p, y_p and x_e, y_e , we know that x, y is bounded. Then from Equation (3.7) and the boundedness of z_1, ψ is also bounded. From Equations (3.7), (3.13b) and the boundedness of z_1 and y_1, r is bounded. Moreover, from the boundedness of z_3, z_4 and u_d, v_d , we know u and v are bounded. Because $\tilde{\lambda}_r, \tilde{\lambda}_u, \tilde{\lambda}_v$ are bounded, we know that the estimated values $\hat{\lambda}_r, \hat{\lambda}_u, \hat{\lambda}_v$ are bounded. Similarly, because $\tilde{W}_r, \tilde{W}_u, \tilde{W}_v$ are bounded, $\hat{W}_r, \hat{W}_u, \hat{W}_v$ are bounded. Finally, all signals in the closed-loop system of fully actuated surface vessel path following are consistent and ultimately bounded.

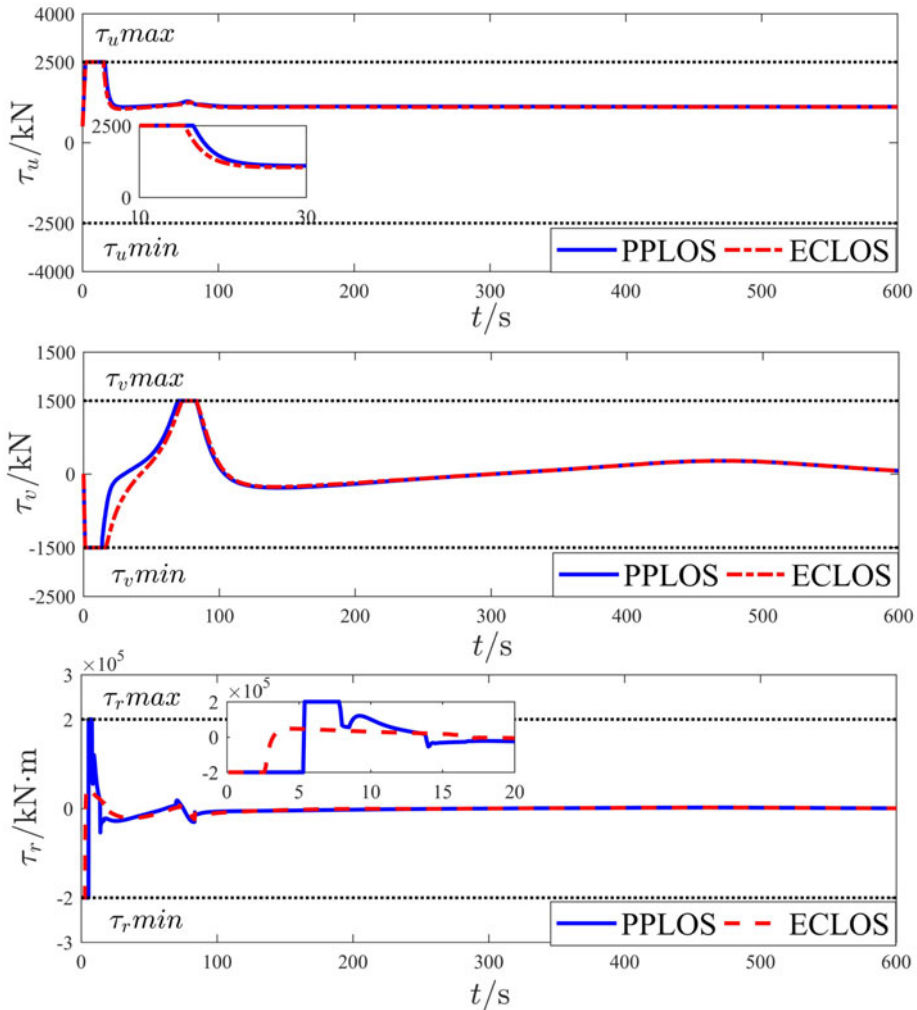


Figure 16. Input signal of sin curve path following.

5. Simulations

To verify the effectiveness of the designed controller, this paper adopts a 76 · 2 m supply surface vessel (Fossen and Strand, 1999) as the object for path following control simulation experiments, and two sets of simulations are carried out. The positive definite inertia matrix, Coriolis centripetal matrix **M** and damping matrix **C(v)** are in Table 1.

The external environmental disturbance **d** and model uncertainties Δ_f are

$$\mathbf{d} = \begin{bmatrix} d_u \\ d_v \\ d_r \end{bmatrix} = 10^3 \times \begin{bmatrix} \sin(0.2 \times t) + \cos(0.5 \times t) \\ \sin(0.1 \times t) + \cos(0.4 \times t) \\ \sin(0.5 \times t) + \cos(0.3 \times t) \end{bmatrix}$$

$$\Delta_f = \begin{bmatrix} 0.2 \times 5 \cdot 0242 \times 10^3 u^2 + 0.1 \times 5 \cdot 0242 \times 10^3 u^3 \\ 0.2 \times 2 \cdot 7299 \times 10^5 v^2 + 0.1 \times 2 \cdot 7299 \times 10^5 v^3 \\ 0.2 \times 4 \cdot 1894 \times 10^8 r^2 + 0.1 \times 4 \cdot 1894 \times 10^8 r^3 \end{bmatrix}$$

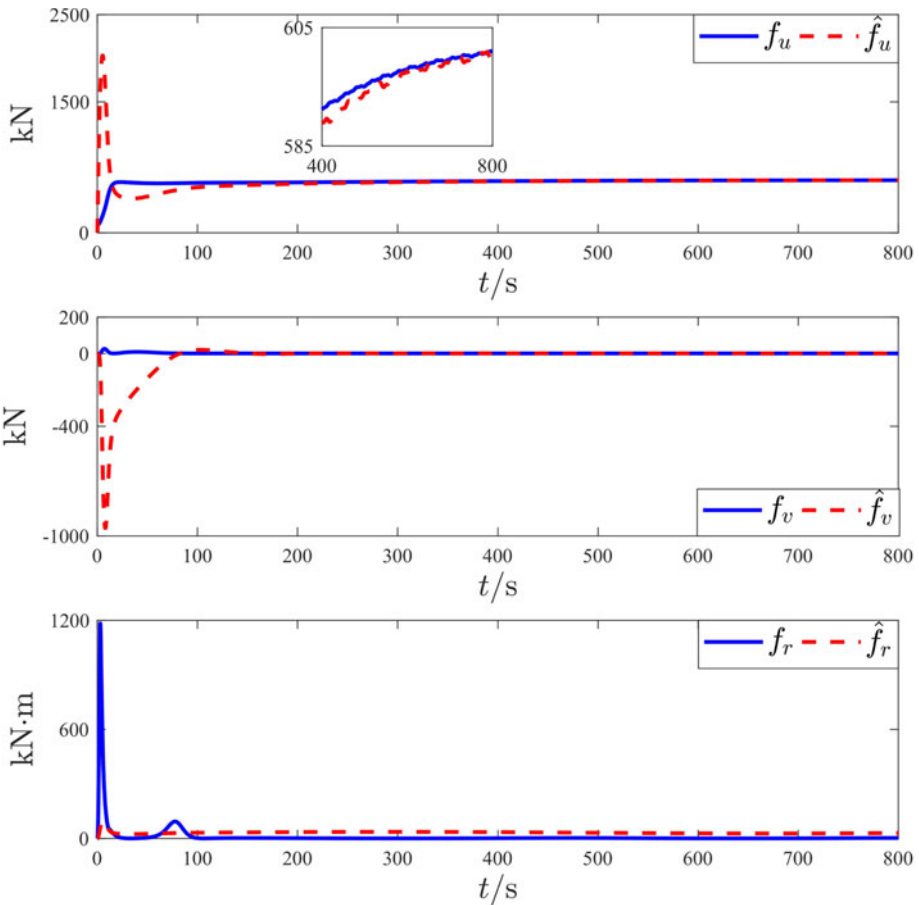


Figure 17. Approximation curves of model uncertainties of sin curve path following.

The neural network has 61 hidden nodes, and the $c_{j,1}$ and $c_{j,2}$ are evenly distributed in the interval $[-18, 18]$, $b_{1,j} = b_{2,j} = 3$, $b_{3,j} = 1$, $j = 1, \dots, 61$ and the initial value of the network weight estimation is 0. The range of system input saturations is $\tau_r \in [-2 \times 10^5, 2 \times 10^5]$ (kN · m), $\tau_u \in [-2 \cdot 5 \times 10^3, 2 \cdot 5 \times 10^3]$ (kN), $\tau_v \in [-1 \cdot 5 \times 10^3, 1 \cdot 5 \times 10^3]$ (kN). The other control parameters of the surface vessel simulation are in Table 2.

In addition, we will give the following simulation comparison. The comparative guidance adopts the ECLOS (Zheng et al., 2018b). In this paper, we choose Equation (3.4) as the desired heading angle ψ_d , and choose Equations (3.3) and (3.1) as the update law of θ where $k_{cs} = 1500$, $k_{ce} = 800$. For better comparison, we use the same surface vessel model, model uncertainties and disturbances. The remaining parameters are the same.

5.1. Straight line path following

In this simulation, the desired straight line path is $\eta_p = [x_p, y_p]^T = [\theta, \theta]^T$, the desired velocities are $[u, v] = [10, 0]$, and the initial position and velocity of the surface vessel are

$$[x(0), y(0), \psi(0), u(0), v(0), r(0)]^T = [100 \text{ m}, 1000 \text{ m}, 0 \text{ rad}, 5 \text{ m/s}, 0 \text{ m/s}, 0 \text{ rad/s}]^T$$

The prescribed performance functions used in straight line path following are in Table 3.

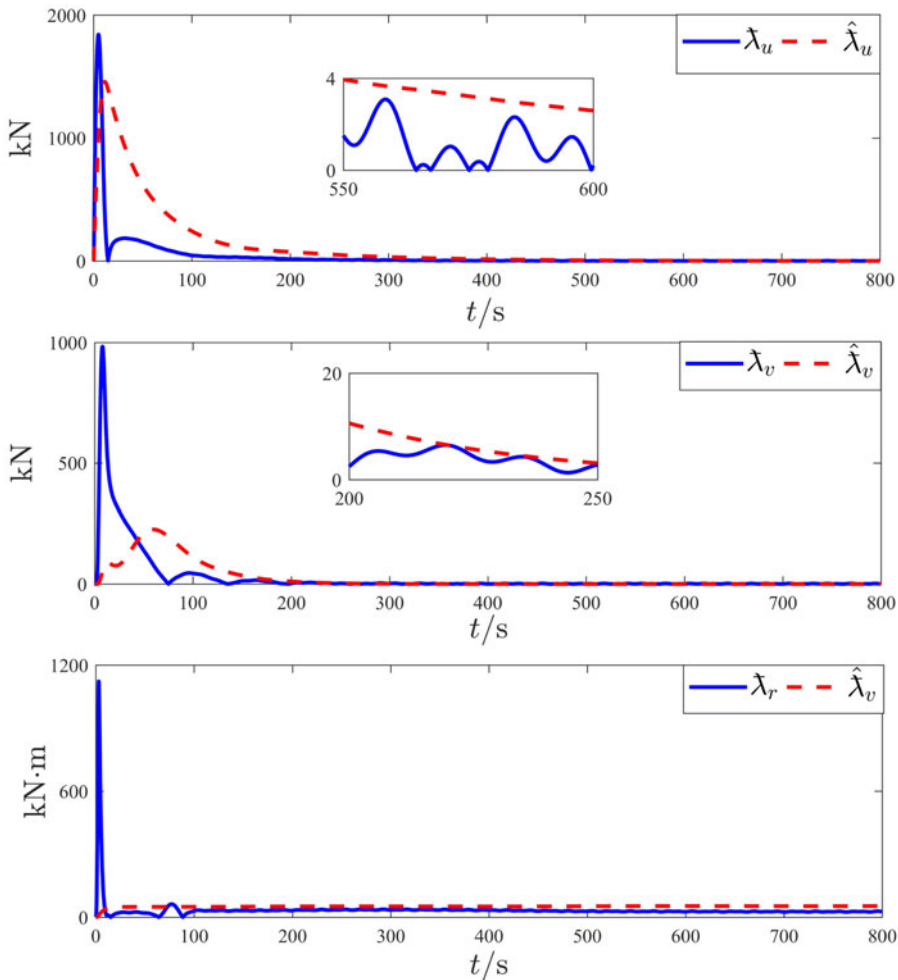


Figure 18. Curves of the bounds of the compound disturbances and its estimation.

The straight line path following simulation results on the proposed PPLOS and comparison with the ECLOS (Zheng et al., 2018b) method are demonstrated in Figures 5–11. Figure 5 displays the straight line path following curves. It shows that, compared with ECLOS guidance using the traditional tan-type BLF, the prescribed performance path following controller of PPLOS guidance based on the PPAMBLF can make the surface vessel reach the desired path quicker and more accurately, and the steady-state error is reduced to a certain extent. Figure 6 shows the long-track error and the across-track error of straight line path following curves. It illustrates that compared with the ECLOS, the path tracking error of PPLOS completely converges within the prescribed performance requirements, which improves the transient performance and steady-state performance of the system. From Figure 7, we can see that the guidance desired heading angle calculated by PPLOS is slightly better, which can make the ship follow the desired path slightly sooner. Moreover, the heading angle error is also within the prescribed performance requirements, the convergence speed is greater and the steady-state error is a little smaller. Figure 8 shows the actual velocity of straight line path following. It can be seen that the surge, sway and yaw of the surface vessel can quickly track the desired velocity. The input signal of straight line path following is presented in Figure 9, which shows that the input signal is within the preset saturation range, so the system can remain stable. The neural network curves are shown in Figure 10, which shows that the model uncertainties can be estimated around 100 s of the straight line path following. Furthermore,

Figure 11 shows the curves of the bounds of the compound disturbance and its estimation. It is obvious that the adaptive laws can approach the bound of compound disturbance.

5.2. Sin curve path following

The desired sin curve path is $\eta_p = [x_p, y_p]^T = [10\theta, 500 \sin(0.01\theta)]^T$, the desired velocities are $[u, v] = [10, 0]$, the initial position and velocity of the surface vessel are

$$[x(0), y(0), \psi(0), u(0), v(0), r(0)]^T = [500 \text{ m}, 1000 \text{ m}, 0 \text{ m/s}, 5 \text{ m/s}, 0 \text{ rad/s}]^T$$

The prescribed performance functions used in sin curve path following are in Table 4.

The sin curve path following simulation results on the proposed PPLOS and comparison with the ECLOS method are demonstrated in Figures 12–18. The sin curve path following curves are shown in Figure 12, from which we can see the method in this paper can ensure that the surface vessel reaches the desired path sooner, and the steady-state error is reduced to a certain extent. As shown in Figure 13, when tracking more complex sin curves, the long-track error and the across-track error can also completely converge within the prescribed performance requirements. Compared with ECLOS, PPLOS slightly improves the transient performance and steady-state performance. From Figure 14, we can see that the PPLOS guidance desired heading angle is better, which can make the ship follow the desired path sooner. In addition, the heading angle error is also within the prescribed performance requirements. It converges slightly faster and its steady-state error is slightly smaller. Furthermore, Figure 15 shows the actual velocity of sin curve path following. The surge, sway and yaw of surface vessel can quickly track the desired velocity. Figure 16 displays the input signal of sin curve path following, which shows that the input signal is within the preset saturation range, while the system can remain stable. Figure 17 shows the neural network curves, and the model uncertainties can be estimated around 100 s of the sin curve path following. As shown in Figure 18, the curves of the bounds of the compound disturbances and their estimation, we can see the adaptive laws can approach the bound of compound disturbance. Consequently, we can conclude that the PPLOS-based path following controller proposed in this paper can track the desired path quicker, and has smaller steady-state errors and better transient performance.

6. Conclusion

In this paper, aimed at the path following control problem of a fully actuated surface vessel, for the system to meet the prescribed performance requirements, we have further improved on the basis of ECLOS and proposed the PPLOS guidance. The guidance is based on the PPAMBLF, which can well converge the position error of path following within the prescribed performance requirements, and improve the steady-state performance and transient performance of the system. Furthermore, the PPAMBLF is also applied to the heading control of surface vessel path following, which can further constrain the heading angle error. We use the backstepping and dynamic surface technique to design the surface vessel path following controller. Furthermore, adaptive assistant systems are constructed to compensate the influence of input saturation on the system, which make the system stable with input saturation. Considering the model uncertainties and the external environment disturbances, the neural network is used to approximate the model uncertainties. At the same time, the neural network approximation errors and external disturbance are combined into compound disturbances, and the upper bound of the compound disturbances are approximated by the adaptive law. The proposed path following controller can guarantee that all signals are semi-globally uniformly ultimately bounded. Finally, the experimental results show the effectiveness of the proposed control in this paper which restricts the steady-state and transient performance of the system.

Acknowledgements. The authors are grateful to the editors and reviewers for their comments, which have improved the quality of this study. This work was supported in part by National Natural Science Foundation of China under Grant 51809028 and Grant 51879027, in part by the China Postdoctoral Science Foundation under Grant 2020M670733, in part by the Doctoral Start-up

Foundation of Liaoning Province under Grant 2019-BS-022 and in part by the Fundamental Research Funds for the Central Universities under Grant 3132019318.

Competing interest. The authors declare that they have no personal competition or interest relationship that could have influence the work reported in this paper.

Authors contribution. Z.S. – Conceptualisation and supervision; A.L. – Writing-original draft, Writing-review and editing; L.L. – Resources; H.Y. – Funding acquisition, Writing-review and editing.

References

- Bechlioulis, C. P. and Rovithakis, G. A.** (2008). Prescribed performance adaptive control of SISO feedback linearizable systems with disturbances. *2008 Mediterr. Conf. Control Autom. - Conf. Proceedings, MED'08*, 1035–1040. Available at: <https://doi.org/10.1109/MED.2008.4601971>.
- Chen, M., Ge, S. S. and Ren, B.** (2011). Adaptive tracking control of uncertain MIMO nonlinear systems with input constraints. *Automatica*, **47**(3), 452–465. doi:10.1016/j.automatica.2011.01.025
- Chen, Z. T., Chen, Q., Sun, M. X. and He, X. X.** (2020). Full state constrained output feedback control for rigid spacecraft. *Control Theory and Applications*, **37**(2), 355–364. doi:10.7641/CTA.2019.80657
- Del-Rio-Rivera, F., Ramirez, V., Donaire, A. and Ferguson, J.** (2020). Robust trajectory tracking control for fully actuated marine surface vehicle. *IEEE Access*, **8**, 223897–223904. doi:10.1109/ACCESS.2020.3042091
- Du, J., Hu, X., Krstić, M. and Sun, Y.** (2016). Robust dynamic positioning of ships with disturbances under input saturation. *Automatica*, **73**, 207–214. doi:10.1016/j.automatica.2016.06.020
- Fossen, T. I. and Berge, S. P.** (1997). Nonlinear vectorial backstepping design for global exponential tracking of marine vessels in the presence of actuator dynamics. *Proceedings of the IEEE Conference on Decision and Control*. Vol. 5, 4237–4242. Available at: <https://doi.org/10.1109/cdc.1997.649499>.
- Fossen, T. I. and Lekkas, A. M.** (2017). Direct and indirect adaptive integral line-of-sight path-following controllers for marine craft exposed to ocean currents. *International Journal of Adaptive Control and Signal Processing*, **31**(4), 445–463. doi:10.1002/acs.2550
- Fossen, T. I. and Strand, J. P.** (1999). Passive nonlinear observer design for ships using Lyapunov methods: full-scale experiments with a supply vessel. *Automatica*, **35**(1), 3–16. doi:10.1016/S0005-1098(98)00121-6
- Hou, Q., Ma, L., Ding, S., Yang, X. and Chen, X.** (2020). Composite finite-time straight-line path-following control of an underactuated surface vessel. *Journal of the Franklin Institute*, **357**(16), 11496–11517. doi:10.1016/j.jfranklin.2019.07.020
- Jia, Z., Hu, Z. and Zhang, W.** (2019). Adaptive output-feedback control with prescribed performance for trajectory tracking of underactuated surface vessels. *ISA Transactions*, **95**, 18–26. doi:10.1016/j.isatra.2019.04.035
- Lekkas, A. M. and Fossen, T. I.** (2014). Integral LOS path following for curved paths based on a monotone cubic hermite spline parametrization. *IEEE Transactions on Control Systems Technology*, **22**(6), 2287–2301. doi:10.1109/TCST.2014.2306774
- Li, Y. and Zheng, J.** (2020). Research on real-time obstacle avoidance planning for an unmanned surface vessel based on the grid cell mechanism. *Journal of Navigation*, **73**(6), 1358–1371. doi:10.1017/S0373463320000338
- Li, J., Du, J., Sun, Y. and Lewis, F. L.** (2019). Robust adaptive trajectory tracking control of underactuated autonomous underwater vehicles with prescribed performance. *International Journal of Robust Nonlinear Control*, **29**(14), 4629–4643. doi:10.1002/rnc.4659
- Liang, J., Zhang, J., Ma, Y. and Zhang, C.-Y.** (2017). Derivation of bathymetry from high-resolution optical satellite imagery and USV sounding data. *Marine Geodesy*, **40**, 466–479. doi:10.1080/01490419.2017.1370044
- Liu, L., Wang, D. and Peng, Z.** (2016a). ESO-based line-of-sight guidance law for straight line path following with exact sideslip compensation. *Proceedings of the World Congress on Intelligent Control and Automation*, 2016-September, 677–681. Available at: <https://doi.org/10.1109/WCICA.2016.7578426>.
- Liu, L., Wang, D., Peng, Z. and Wang, H.** (2016b). Predictor-based LOS guidance law for path following of underactuated marine surface vehicles with sideslip compensation. *Ocean Engineering*, **124**, 340–348. doi:10.1016/j.oceaneng.2016.07.057
- Liu, C., Chen, C. L. P., Zou, Z. and Li, T.** (2017). Adaptive NN-DSC control design for path following of underactuated surface vessels with input saturation. *Neurocomputing*, **267**, 466–474. doi:10.1016/j.neucom.2017.06.042
- Lyu, H. and Yin, Y.** (2019). COLREGS-constrained real-time path planning for autonomous ships using modified artificial potential fields. *Journal of Navigation*, **72**(3), 588–608. doi:10.1017/S0373463318000796
- Naus, K., Waqz, M., Szymak, P., Gućma, L. and Gućma, M.** (2021). Assessment of ship position estimation accuracy based on radar navigation mark echoes identified in an electronic navigational chart. *Measurement*, **169**, 108630. doi:10.1016/j.measurement.2020.108630
- Nie, J., Wang, H., Lu, X., Lin, X., Sheng, C., Zhang, Z. and Song, S.** (2021). Finite-time output feedback path following control of underactuated MSV based on FTESO. *Ocean Engineering*, **224**, 108660. doi:10.1016/j.oceaneng.2021.108660
- Qiu, Y., Liang, X., Dai, Z., Cao, J. and Chen, Y.** (2015). Backstepping dynamic surface control for a class of non-linear systems with time-varying output constraints. *IET Control Theory and Applications*, **9**(15), 2312–2319. doi:10.1049/iet-cta.2015.0019
- Rutkowski, G.** (2021). Analysis of a practical method for estimating the ship's best possible speed when passing under bridges or other suspended obstacles. *Ocean Engineering*, **225**, 108790. doi:10.1016/j.oceaneng.2021.108790

- Shen, Z., Zhang, X., Zhang, N. and Guo, G. (2018). Recursive sliding mode dynamic surface output feedback control for ship trajectory tracking based on neural network observer. *Control Theory and Applications*, **35**(8), 1092–1100. doi:10.7641/CTA.2018.70456
- Shen, Z., Bi, Y., Wang, Y. and Guo, C. (2020a). MLP neural network-based recursive sliding mode dynamic surface control for trajectory tracking of fully actuated surface vessel subject to unknown dynamics and input saturation. *Neurocomputing*, **377**, 103–112. doi:10.1016/j.neucom.2019.08.090
- Shen, Z., Wang, Y., Yu, H. and Guo, C. (2020b). Finite-time adaptive tracking control of marine vehicles with complex unknowns and input saturation. *Ocean Engineering*, **198**, 106980. doi:10.1016/j.oceaneng.2020.106980
- Specht, M., Stateczny, A., Specht, C., Widźgowski, S., Lewicka, O. and Wiśniewska, M. (2021). Concept of an innovative autonomous unmanned system for bathymetric monitoring of shallow waterbodies (INNOBAT system). *Energies*, **14**, 5370. doi:10.3390/en14175370
- Stateczny, A., Specht, C., Specht, M., Brčić, D., Jugović, A., Widźgowski, S., Wiśniewska, M. and Lewicka, O. (2021). Study on the positioning accuracy of GNSS/INS systems supported by DGPS and RTK receivers for hydrographic surveys. *Energies*, **14**, 7413. doi:10.3390/en14217413
- Swaroop, D., Hedrick, J. K., Yip, P. P. and Gerdes, J. C. (2000). Dynamic surface control design for a class of nonlinear systems. *IEEE Trans. Automat. Contr.*, **45**(10), 1893–1899. doi:10.1109/TAC.2000.880994
- Wang, N. and Su, S. F. (2021). Finite-time unknown observer-based interactive trajectory tracking control of asymmetric underactuated surface vehicles. *IEEE Transactions on Control Systems Technology*, **29**(2), 794–803. doi:10.1109/TCST.2019.2955657
- Wang, N., Sun, Z., Yin, J., Zou, Z. and Su, S. F. (2019). Fuzzy unknown observer-based robust adaptive path following control of underactuated surface vehicles subject to multiple unknowns. *Ocean Engineering*, **176**, 57–64. doi:10.1016/j.oceaneng.2019.02.017
- Wang, Y., Shen, Z., Wang, Q. and Yu, H. (2021). Predictor-based practical fixed-time adaptive sliding mode formation control of a time-varying delayed uncertain fully-actuated surface vessel using RBFNN. *ISA Transactions*. doi:10.1016/j.isatra.2021.06.021
- Xie, W., Reis, J., Cabecinhas, D. and Silvestre, C. (2020). Design and experimental validation of a nonlinear controller for underactuated surface vessels. *Nonlinear Dynamics*, **102**(4), 2563–2581. doi:10.1007/s11071-020-06058-8
- Xu, J. X. and Jin, X. (2013). State-constrained iterative learning control for a class of MIMO systems. *IEEE Transactions on Automatic Control*, **58**(5), 1322–1327. doi:10.1109/TAC.2012.2223353
- Xu, X., Pan, W., Huang, Y. and Zhang, W. (2020). Dynamic collision avoidance algorithm for unmanned surface vehicles via layered artificial potential field with collision cone. *Journal of Navigation*, **73**(6), 1306–1325. doi:10.1017/S0373463320000284
- Yang, Q. and Chen, M. (2016). Adaptive neural prescribed performance tracking control for near space vehicles with input nonlinearity. *Neurocomputing*, **174**, 780–789. doi:10.1016/j.neucom.2015.09.099
- Zhang, G., Zhang, X. and Zheng, Y. (2015). Adaptive neural path-following control for underactuated ships in fields of marine practice. *Ocean Engineering*, **104**, 558–567. doi:10.1016/j.oceaneng.2015.05.013
- Zhang, G., Li, J., Li, B. and Zhang, X. (2019). Improved integral LOS guidance and path-following control for an unmanned robot sailboat via the robust neural damping technique. *Journal of Navigation*, **72**(6), 1378–1398. doi:10.1017/S0373463319000353
- Zhang, C., Wang, C., Wei, Y. and Wang, J. (2020). Robust trajectory tracking control for underactuated autonomous surface vessels with uncertainty dynamics and unavailable velocities. *Ocean Engineering*, **218**, 108099. doi:10.1016/j.oceaneng.2020.108099
- Zhao, Z., He, W. and Ge, S. S. (2014). Adaptive neural network control of a fully actuated marine surface vessel with multiple output constraints. *IEEE Transactions on Control Systems Technology*, **22**(4), 1536–1543. doi:10.1109/TCST.2013.2281211
- Zheng, Z. and Feroskhan, M. (2017). Path following of a surface vessel with prescribed performance in the presence of input saturation and external disturbances. *IEEE/ASME Transactions on Mechatronics*, **22**(6), 2564–2575. doi:10.1109/TMECH.2017.2756110
- Zheng, Z., Huang, Y., Xie, L. and Zhu, B. (2018a). Adaptive trajectory tracking control of a fully actuated surface vessel with asymmetrically constrained input and output. *IEEE Transactions on Control Systems Technology*, **26**(5), 1851–1859. doi:10.1109/TCST.2017.2728518
- Zheng, Z., Sun, L. and Xie, L. (2018b). Error-constrained LOS path following of a surface vessel with actuator saturation and faults. *IEEE Transactions on Systems, Man, and Cybernetics: Systems*, **48**(10), 1794–1805. doi:10.1109/TSMC.2017.2717850